Bulletin of the Seismological Society of America, 90, 3, pp. 545–565, June 2000

Characteristics of Observed Peak Amplitude for Strong Ground Motion from the 1995 Hyogoken Nanbu (Kobe) Earthquake

by Yoshimitsu Fukushima, Kojiro Irikura, Tomiichi Uetake, and Hisashi Matsumoto

Abstract Over 200 peak amplitudes of strong motion were observed at distances of less than 250 km from the fault during the 1995 Hyogo-ken Nanbu (Kobe) earthquake. We analyzed the attenuation of the peak-ground acceleration and velocity as a function of distance and geological site conditions. The observed peak amplitudes agree well with those predicted by an empirical attenuation relation that was developed for Japanese earthquakes. This demonstrates that on average the peak amplitude of the ground motion generated by this damaging earthquake did not exceed the level predicted by the empirical attenuation relation. We found a significant effect of the surface geology on the observed ground-motion peak amplitude. In particular for soft-soil sites, located near the fault, the peak-horizontal acceleration decreases rapidly with distance as a result of the nonlinear response of soils. In order to take into account the effect of the site conditions we introduced correction factors to the existing attenuation relation. This resulted in a significant reduction of the residuals between the predicted and observed peak amplitudes. Based on the attenuation relation corrected for the site condition effect we generated a map of horizontal peak-ground acceleration in the Kobe and Osaka area for the Kobe earthquake. The area of simulated large ground motion agrees well with the severe damage zone of intensity VII, JMA scale.

Introduction

More than 6,500 people were killed and 170,000 buildings were destroyed in the Hanshin and Awaji areas as a result of the 17 January 1995 Hyogo-ken Nanbu earthquake. The origin time and hypocenter of the event given by the Japan Meteorological Agency (JMA) were 05h46m52sec (local time) and longitude 135°2.6′ E, latitude 34°36.4′ N, respectively, and the focal depth was 14.3 km. The magnitude was M_j 7.2 determined by the JMA, M_s 6.8 by the U.S. Geological Survey, and M_w 6.9 by Harvard University and Kikuchi (1995) from a seismic moment of 2.5×10^{26} dyne cm. The JMA intensity was VII throughout a narrow beltlike area stretching from Awaji Island to Nishinomiya City east of Kobe. The surface fault trace in the southwest part of the source area was in evidence along the Nojima fault in the Hokutan-cho area of Awaji island (Nakata *et al.,* 1995). No clear surface trace was found in the eastern part of the source area around Kobe on Honshu island. Shimamoto (1995) presumed the area of JMA intensity VII corresponding to the faults, which generated the earthquake. On the other hand, aftershocks occurred close to existing Quaternary faults, which are located north of Kobe. Sekiguchi *et al.* (1996) identified three fault segments along the Rokko fault system using the particle motions of the strong-motion records and the geodetic data in the near-source region. Kamae *et al.* (1998) and Kamae and Irikura (1998) simulated ground motions from the main shock by an empirical Green's function method using the asperity distribution on the fault founded by Sekiguchi *et al.* (1996). Their simulated ground motions agree well with the observed one. Based on simulated near-fault velocity in the frequency range of 0.1–1.0 Hz, Sekiguchi *et al.* (2000) showed that the eastern end of the source was likely to have branched to the Gosukebashi and Ashiya faults. The precise fault location is still being investigated. In this study we adapted the fault model of Sekiguchi *et al.* (1996). One of the most important issues is whether the disaster resulted from unpredictable strong-ground motion or not. We address this issue in this study by analyzing the attenuation of the ground motion as a function of the closest distance to the fault.

Over 200 peak amplitudes of ground motion were observed during this earthquake. The main purpose of these observations was not to do research work but rather emergency response systems. Individual organizations that had strong-motion data kindly made their data available for this work. We investigated the records and the site conditions in detail. The sensors were installed on various ground conditions and some were located in seriously damaged areas. The observed peak-horizontal acceleration (PHA) and velocity

(PHV) were compared with predicted values using attenuation relations developed in Japan (Fukushima and Tanaka, 1992: modified Fukushima and Tanaka, 1990; Midorikawa, 1993). Similar comparisons have been performed in other studies (e.g., Irikura and Fukushima, 1995; Ejiri *et al.* 1996; Midorikawa *et al.* 1996; Fukushima *et al.* 1997). In this study, the ratio of predicted to observed peak amplitude is newly studied for various ground conditions: (1) bedrock; (2) Neogene; (3) diluvium, which is the consolidated alluvium; (4) alluvium, which is unconsolidated; and (5) reclaimed ground. Further, the ratio of peak vertical acceleration (PVA) and velocity (PVV) to horizontal component is evaluated. The PHA/PHV and PVA/PVV ratios for various ground conditions are also studied.

At several sites close to the source, PVA was higher than PHA on soft soil ground. This phenomenon was previously observed at Array 6 in the 1979 Imperial Valley earthquake, and has been explained in terms of nonlinear behavior (Mohammadioun and Pecker, 1984). Clear nonlinear behavior has been identified in the Kobe event in vertical array records at Port Island, where the PVA at the surface was also larger than the horizontal component.

The determination of spatial distribution for PHA near fault is very important to know the strong ground motion characteristics in the near-source region. Some iso-PHA maps were determined from the observation PHAs only. However, these are usually difficult subjects because the determination of average function is almost equal to deriving a new attenuation relation, which must be applicable to the near source region (Stewart *et al.,* 1994; Borcherdt and Holzer, 1996). Even if an attenuation relation could be used as the average function, the distribution of PHA was distorted in sparse observation area (Fukushima *et al.,* 1998). Fortunately, the digital geological information furnished as the GIS (the Digital National Land Information compiled by the Geographic Survey Institute and the National Land Agency, Japan) around this area is available. We try to derive correction functions of the geological conditions and determine an iso-PHA map multiplying the predicted value by the attenuation relation and the correction function.

Data

Prior to this event, strong-motion data were disclosed by only a few observational organizations in Japan. After the Kobe event, however, all organizations kindly made their data available. Peak-ground accelerations and velocities from the event were announced immediately by the Railway Technical Research Institute (RTRI; Nakamura *et al.,* 1995), Osaka Gas Co., Ltd., the Committee of Earthquake Observation and Research in the Kansai Areas (CEORKA), Kansai Electric Power Company (KEPCO), the Port and Harbor Research Institute (PHRI), the JMA, and others. A database of peak ground accelerations and velocities was compiled from these announcements and a prompt report was published by NIED (National Research Institute for Earth Science and Disaster Prevention, Science and Technology Agency, 1995). Digital records of strong-ground motions from this event were made available to the public by CEORKA (10 sites), JMA (14 sites), and the Port Island Strong Motion Station of the Development Bureau of Kobe city (four sites in a vertical array) within a few weeks. These data were compared with attenuation relations by Irikura and Fukushima (1995) and listed in Fukushima and Irikura (1997).

The catalog for strong-motion data of the earthquake was published by the Architectural Institute of Japan (1996) together with time histories, response spectrum, and particle orbits. The largest number of observation sites belongs to the Japan Railway Companies (JR), and their details were reported in Nakamura *et al.* (1996). The Conference on Usage of Earthquakes (CUE) in RTRI distributed five major records by floppy disks; this study is using the floppy disk with serial number R-031. The JMA distributed records taken by JMA87 type instruments through the Japan Weather Association. PHRI immediately released their records, and they were reported by Miyata *et al.* (1995). Records of the Public Works Research Institute (PWRI) of the Ministry of Construction, Hanshin Expressway Public Corporation, and Honshu-Shikoku Bridge Authority are announced in the Technical Note of PWRI (1995), and their digital data are distributed by floppy disks with the Technical Note. The Building Research Institute (BRI) of the Ministry of Construction reported their data in Kashima and Kitagawa (1995). CEORKA reported on observation records just after the event (Geo-Research Institute, Osaka, 1995). The Japan Society for Earthquake Engineering Promotion (1998) completed a database and distributed it on CD with a report. The CD contains data observed by Obayashi Corporation, Konoike Construction Co., Ltd., Maeda Corporation, KEPCO, Osaka Gas Co. Ltd., RWRI, BRI, PHRI, Ministry of Posts and Telecommunications, Hanshin Expressway Public Corporation, Kobe City Office, Shiga Prefecture, Laboratory of Strong Motion Seismology of DPRI, Research Center of Earthquake Prediction of DPRI of Kyoto University, Research Reactor Institute Kyoto University, and Shiga Prefecture University. Data from other organizations, such as the Ohsaka Technical Institute, Kansai University, NTT, Takenaka, Hankyu Railway, the Technical Institute of Matsumura-gumi, Kansai Airport and others, are listed by the Architectural Institute of Japan (1996). Further, Hokushin Railway, Nose Railway, and NHK announced their data individually.

These strong-motion instruments have been installed for various purposes, so their sensors were set up differently. We investigated the individual site condition of each instrument (Matsumoto *et al.,* 1998). The investigated sites are listed in the appendix.

The peak acceleration and velocity data contain differential values from the velocity records and integral values from the accelerograms, respectively. Although the fault-normal component is already known to be very large in the near-fault region (Somerville *et al.,* 1997), the orientation of

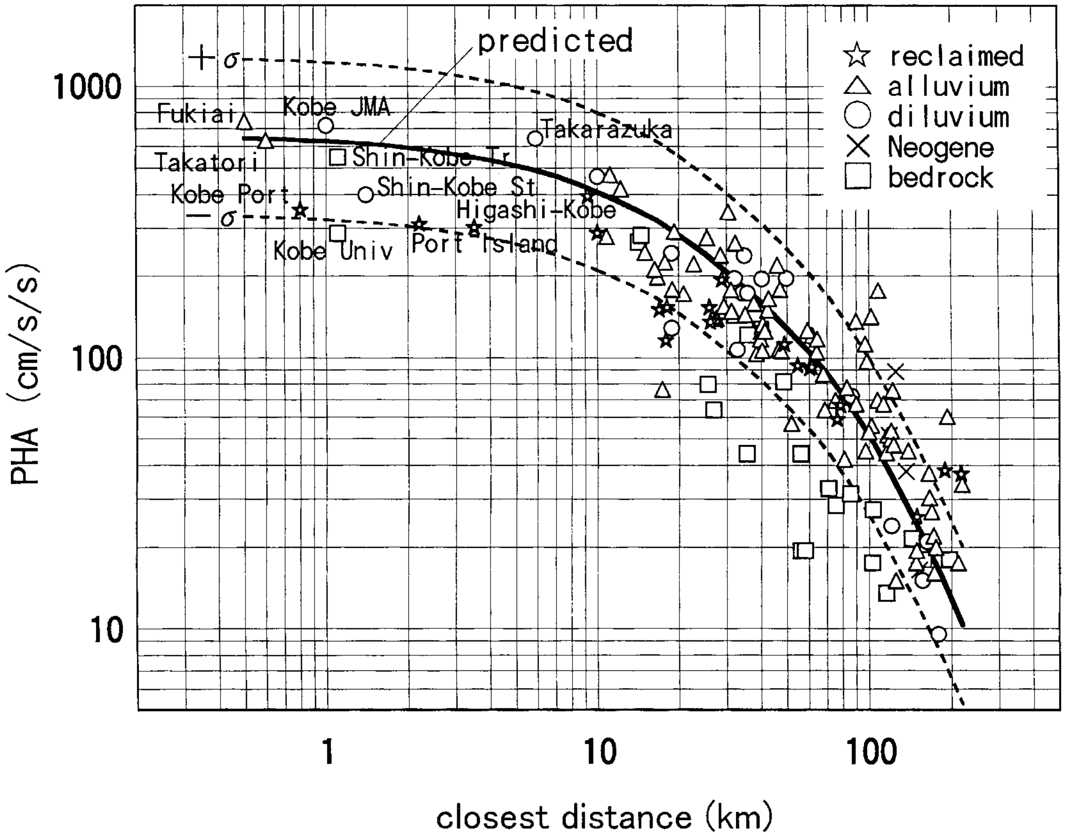

Figure 1. Comparison between observed peak-horizontal accelerations and the predicted values using empirical attenuation equation (1). Individual marks indicate different ground conditions at the observation site. The solid line indicates the predicted peak-horizontal acceleration. Broken lines indicate the standard error of the equation.

Table 1
Number of Data

Category	PHA	PHV	PVA	PVV
Bedrock	22	21	22	19
Neogene	5	↑	4	—
Diluvium	18	13	16	10
Alluvium	76	45	68	39
Reclaimed	21	17	20	15
All data	142	96	130	83

some sites is unknown; therefore, the mean peaks of two horizontal components are taken to be PHA and PHV. Data of only one horizontal component is rejected.

These mean values are more stable and only 10% smaller than the maximum values of the two corresponding horizontal components on average. A total of 142 PHA and 96 PHV observations were selected on the basis of the following conditions:

1. The sensor should be installed on free surface. Sensor located in structures such as buildings were excluded from the study.
2. Borehole instruments installed at a depth greater than 1 m for soil site and greater than few tens of meters for rock site are excluded in order to avoid the effect of the downgoing waves reflected at the ground surface.
3. Only large records are observed at far distance and biased on the average characteristics (Fukushima, 1997). Therefore the records at the distances less than 220 km are accepted. This is the reliability limit of the attenuation relation (Fukushima and Tanaka, 1990) for this magnitude.

The number of PVA and PVV records are 130 and 83, respectively; this number is smaller than the one for PHA, because the absence of vertical sensors at some sites. No surface trace was found in the eastern part of the fault, so it is difficult to precisely locate the fault plane. We assumed a single plane, simplifying the three-segment-fault model of Sekiguchi *et al.* (1996). The length, width, strike angle, and dip angle of the fault plane are assumed to be 45 km, 15 km, 235 degrees, and 85 degrees, respectively. The shortest distance from the simplified fault model to the observation site is used for empirical predictions of peak amplitude in this study. Because fault distance errors are up to several hundred meters, estimated distances of less than 500 m were taken to be 500 m. Ground conditions at individual observation

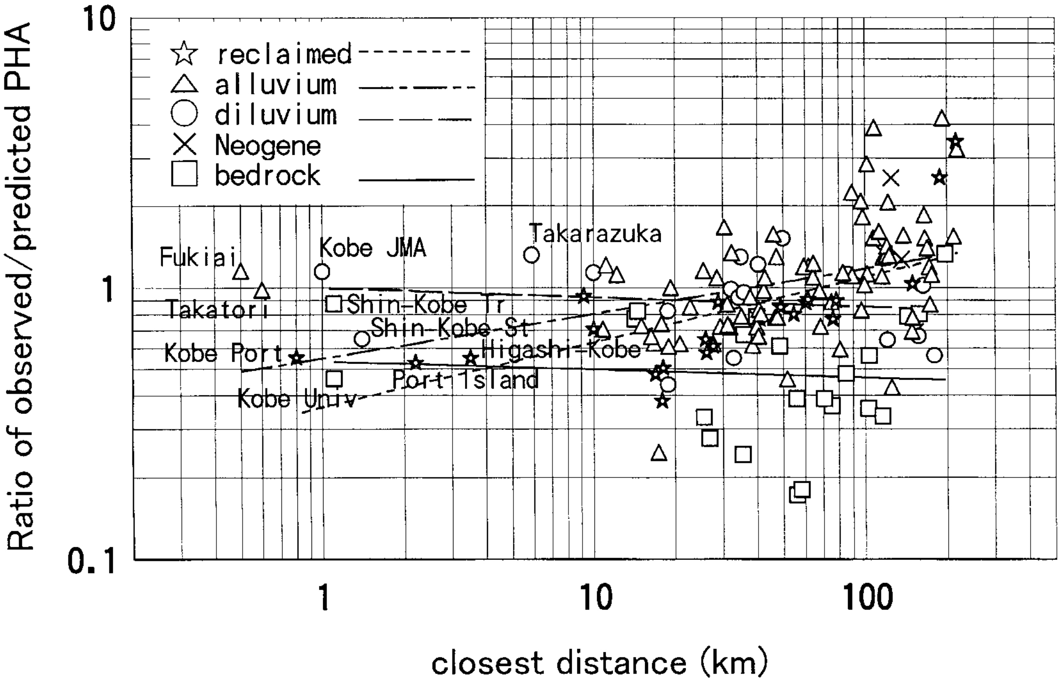

Figure 2. Relation between ratio of observed to predicted peak-horizontal acceleration and closest distance to the fault plane. Individual marks indicate different ground conditions at the observation site. Regression lines on the logarithmic scale are also indicated for the individual ground conditions.

Table 2
Ratios of Peak Amplitudes

	Average in linear scale					
Category	Observed/Predicted PHA	Observed/Predicted PHV	PVA/PHA	PVV/PHV	PHA/PHV	(PVA/PVV)/(PHA/PHV)
Bedrock	0.55	0.59	0.59	0.49	9.6	1.3
Neogene	few data	↑	0.30	—	—	—
Diluvium	0.94	0.78	0.46	0.38	13.5	1.3
Alluvium	distance dependent	1.16	0.45	0.33	10.4	1.5
Reclaimed	distance dependent	0.86	0.77	0.40	8.4	2.3
All data	1.03	0.93	0.53	0.39	10.4	1.6

sites were investigated from geological maps and logging data in the site vicinity and confirmed by visits to the site. Geological site conditions are classified into five types: (1) seismic bedrock, e.g., sedimentary rock predating the Neogene, and volcanic or plutonic rock; (2) Neogene strata; (3) diluvium; (4) alluvium; and (5) reclaimed ground. The number of data points in each category is indicated in Table 1. There is only one observation of PHV on the Neogene, therefore, this data is included in the bedrock category.

Attenuation Relations

Fukushima and Tanaka (1990) collected 686 PHAs from 28 earthquakes in Japan and 15 earthquakes in the United States and other countries and used them to develop an attenuation relation by a two-step regression analysis. Later, new data of 147 PHAs were added and the attenuation relation was revised. The new result was almost the same as the previous one (Fukushima and Tanaka, 1992). This indicates that the derived empirical attenuation relation is very stable. The relation is given in the form of the following equation:

$$\log \mathrm{PHA} = 0.42M_w - \log(R + 0.025 \times 10^{0.42M_w}) - 0.0033R + 1.22 \quad (1)$$

where, PHA is in cm/sec^2, M_W is the moment magnitude, and R is the distance from the fault plane to the site in km. Ground conditions at the individual observation sites were not classified; therefore, this equation may be taken as corresponding to average ground conditions in Japan.

Recently, a nonlinear scaling between earthquake ground motion and M_W has been recognized (Fukushima, 1996), particularly in the predominant period of several seconds, which is effective to PHV. In addition, a strong dependence on average S-wave velocity near the ground surface can be seen in PHV. Taking this nonlinear scaling and the dependence on S-wave velocity into account, Midorikawa (1993) developed the following attenuation relation for PHV:

$$\log \mathrm{PHV} = -0.22M_w^2 + 3.94M_w - \log(R + 0.01 \times 10^{0.43M_w}) - 0.002R - 11.9 - 0.71 \times \log V_s \quad (2)$$

where, PHV is in cm/sec and V_S is the average S-wave velocity from the surface to 30 m deep in m/sec.

Amplitude Ratios

Observed/Predicted

Predicted PHA values from equation (1) are compared with the observed values in Figure 1. Most of the observed data points fall within the standard error of the attenuation relation, even if errors of several hundred meters in evaluating the distance from the fault are considered. The ratios of observed/predicted PHA are shown in Figure 2 with different marks for individual geological conditions. As shown in Table 2, the average ratios for bedrock and diluvium are 0.55 and 0.94. At distance ranges over 100 km, the ratios for alluvium and reclaimed ground are larger than 1.0 on average. On the contrary, the ratios for reclaimed ground and alluvium decrease with decreasing distance due to the nonlinear behavior of soils described in the next section. The following equations are adopted as the distance dependent ratios for the reclaimed ground and alluvium:

$$\mathrm{O/P(reclaimed)} = 0.362 \times R^{0.241} \quad (3)$$

$$\mathrm{O/P(alluvium)} = 0.549 \times R^{0.165} \quad (4)$$

where O/P is observed/predicted PHA ratio. Using these correction factors, the standard error decreases from 0.247 to 0.193 in base-ten logarithms. Further, if these distance dependencies are caused by nonlinear behavior, the level of PHA may affect the ratio. Figure 3 shows the relation between the ratio of observed to predicted PHA and the predicted PHA. The following relations between predicted PHA and the ratio are determined for reclaimed ground and alluvium:

$$\mathrm{O/P(reclaimed)} = 5.476 \times \mathrm{PHA}^{-0.383} \quad (5)$$

$$\mathrm{O/P(alluvium)} = 3.113 \times \mathrm{PHA}^{-0.239} \quad (6)$$

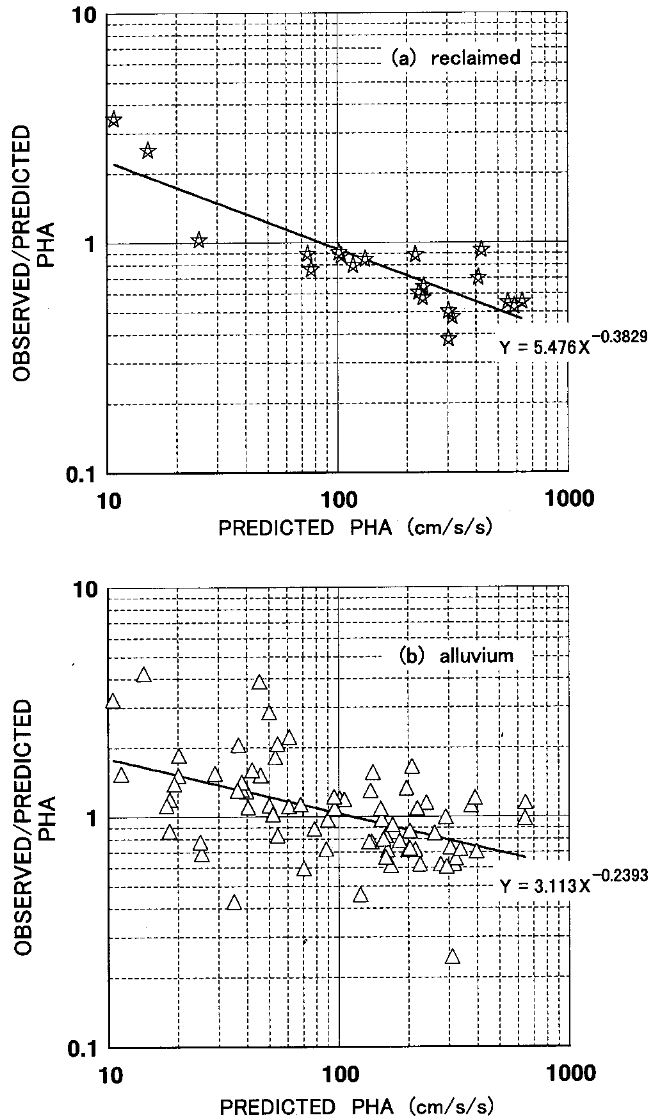

Figure 3. Relation between ratio of observed to predicted peak-horizontal acceleration and the predicted peak-horizontal acceleration for (a) reclaimed ground and (b) alluvium. Solid lines indicate regression lines for the data points.

Using these correction factors, the standard error decreases to 0.180. Although it is limited to the case of the Hyogo-ken Nanbu event, this residual corresponds to a standard deviation from 66% to 151% for predicted PHA.

The comparison between observed and predicted PHVs is shown in Figure 4. In this figure, the prediction curves for the reference S-wave velocity (hereafter V_S) of 400 m/sec, which is an average V_S of the database of Midorikawa (1993), as well as those for 200 and 700 m/sec are indicated for a comparison of different values of V_S. Equation (2) agrees well with the data. The ratios of observed/predicted PHV for the individual geological conditions are shown in Figure 5. As shown in Table 2, the ratios for stiff ground on average are small, for example, about 0.59 for bedrock and

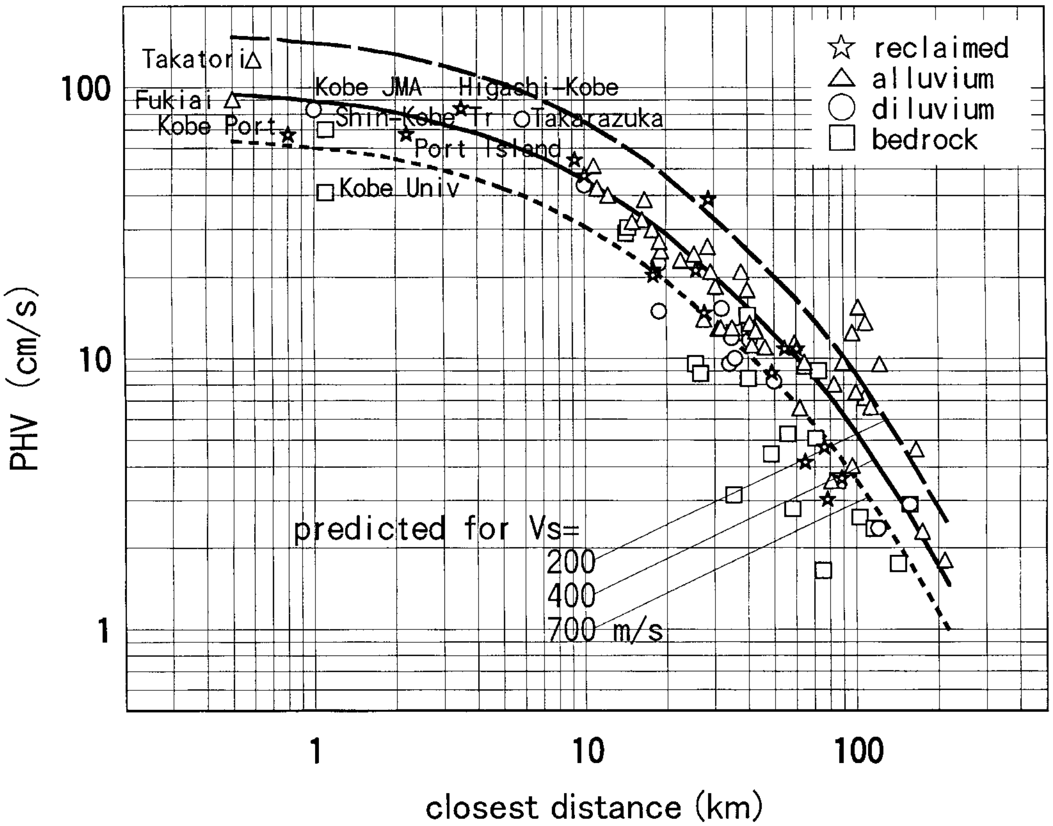

Figure 4. Comparison between observed peak-horizontal velocities and predicted levels using empirical attenuation equation (2). Individual marks indicate different ground conditions at the observation site. The predicted peak horizontal velocity for a reference V_S of 400 m/sec is indicated by the solid line. The predicted velocities for other V_S of 200 and 700 m/sec are also indicated by broken and chained lines, respectively.

0.78 for diluvium. The distance dependence seen in the case of PHA for soft soils cannot be seen in the case of PHV.

Vertical/Horizontal

The ratios of PVA/PHA are shown in Figure 6. In this figure, the dispersion in the data is too large to allow a systematic discussion. The average ratio is 0.53 as shown in Table 2. Most cases where the ratio is larger than 1.0 correspond with reclaimed ground or alluvium. All of these points are located near the seashore. This may be due to the effects of the nonlinear behavior, which was similarly observed during the 1979 Imperial Valley, California, earthquake (Mohammadioun and Pecker, 1984). Kawase *et al.* (1995) interpreted the remarkable decay of the horizontal components at the surface using effective stress analysis for the vertical array records at Port Island. Namely, the high-frequency horizontal component propagating as a shear wave was isolated by the liquefied soil. On the contrary, the high-frequency vertical component propagating as a compressional wave was amplified by the large contrast in *P*-wave velocity at the ground water level.

The ratios of PVV/PHV are shown in Figure 7. All ratios are less than 1.0 and their average is 0.39. The ratios for bedrock seem to be larger than those for the other categories. This might be due to the large incident angle of *SV* wave to the bedrock. However, even for bedrock, the average ratio is less than 0.5. The peak acceleration correlates with the response spectral intensity of the predominant period from 0.2 to 0.8 seconds, whereas the peak velocity correlates with a relatively long period range from 0.5 to 1.5 seconds (Nakazawa *et al.,* 1998). Therefore, the nonlinear behavior has less effect on the peak velocity than on acceleration.

Acceleration/Velocity

The average ratio of PHA/PHV for the observed data shown in Table 2 is 10. As shown in Figure 8, the individual ratios have a remarkable dependence on distance. The ratio peaks at around 50 km. Values of PHA/PHV predicted from equations (1) and (2) are also shown in this figure. The curve of the predicted ratio has a similar characteristic. This fact indicates that the bend of attenuation curve for PHA is sharper than that for PHV around 50 km. The observed ratios for soft soil in the distance range less than 10 km are small due to the decrease in PHA caused by the nonlinear behavior

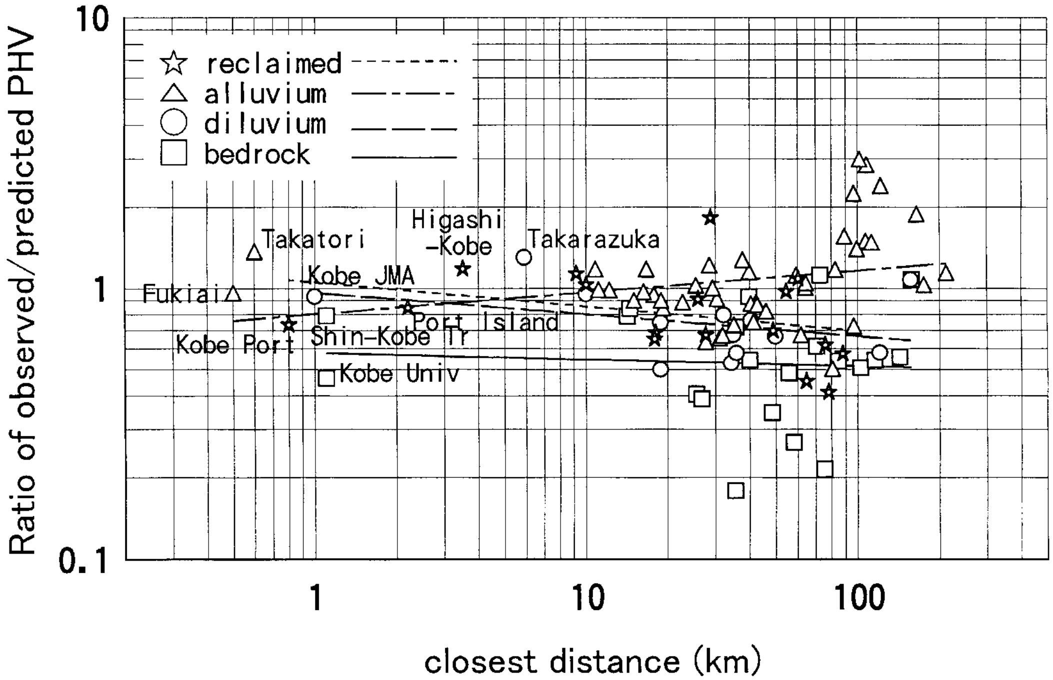

Figure 5. Relation between ratio of observed to predicted peak horizontal velocity for V_S 400 m/sec and closest distance to the fault plane. Individual marks indicate different ground conditions at the observation site. Regression lines on the logarithmic scale are also indicated for the individual ground conditions.

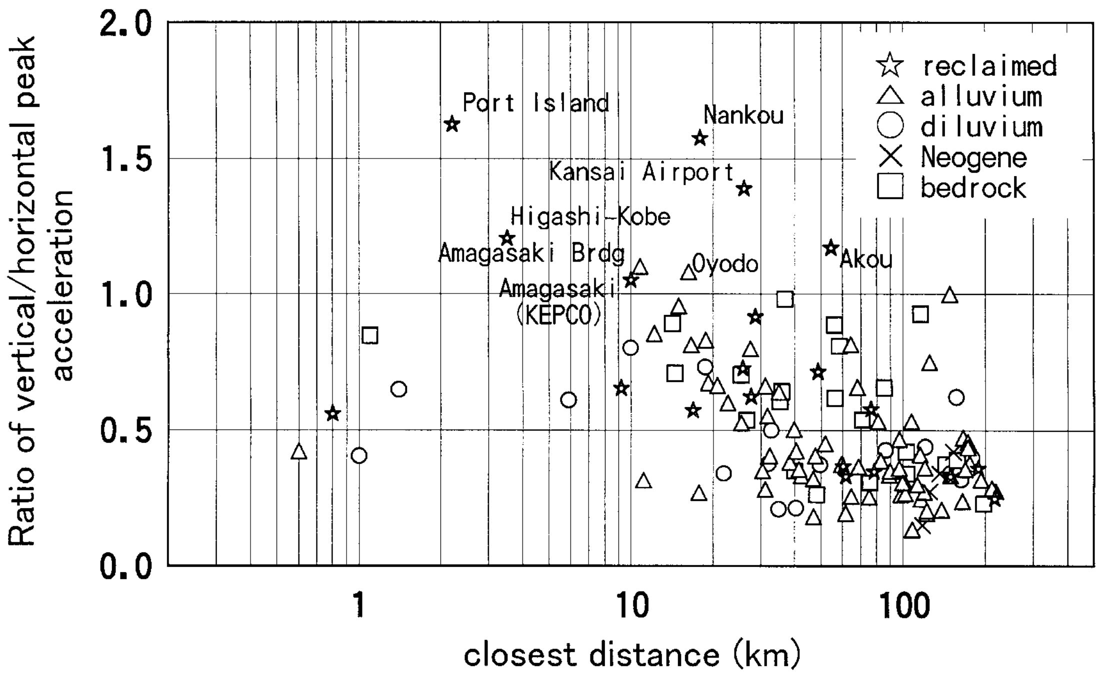

Figure 6. Relation between ratio of observed peak vertical per horizontal acceleration and distance. Individual marks indicate different ground conditions at the observation site.

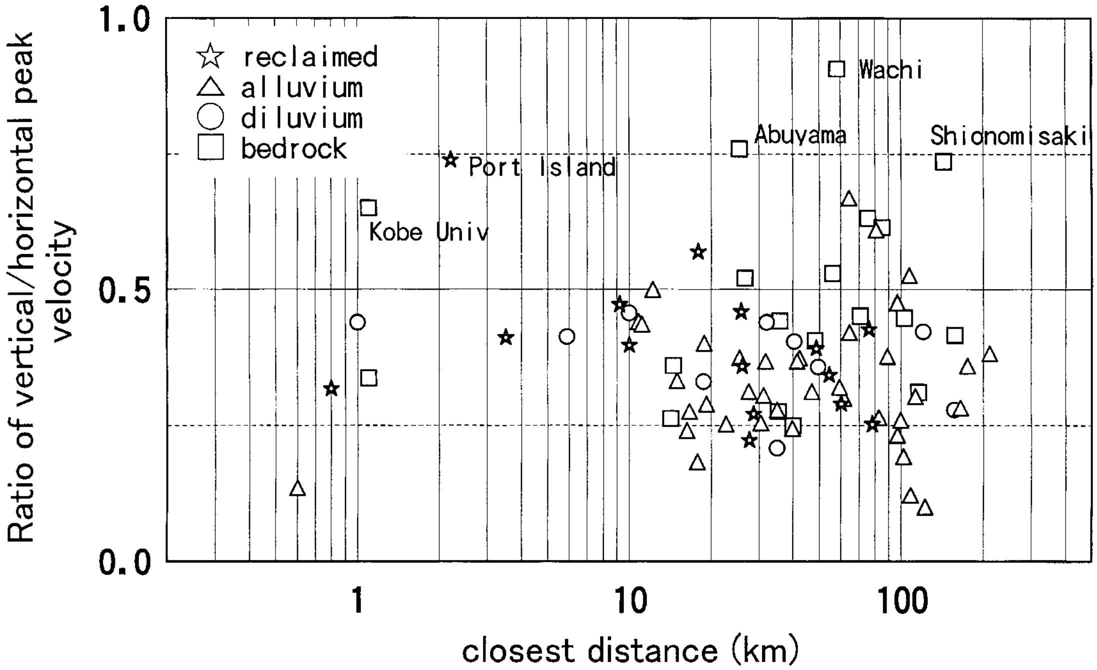

Figure 7. Relation between ratio of observed peak vertical to horizontal velocity and distance. Individual marks indicate different ground conditions at the observation site.

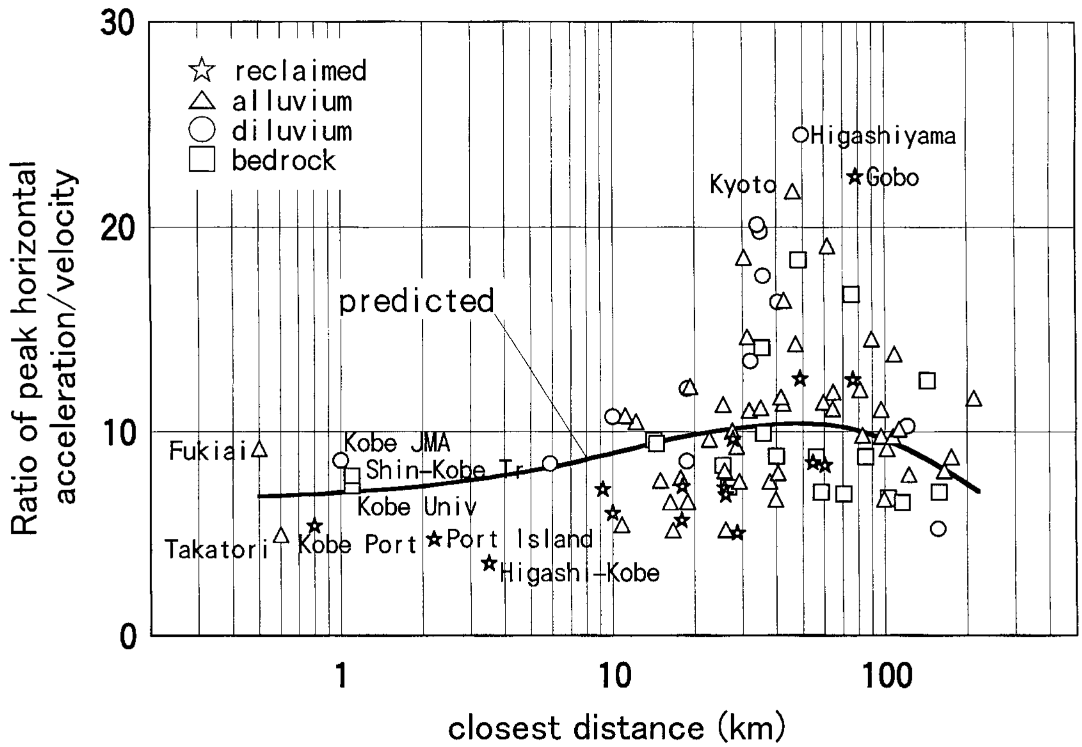

Figure 8. Ratio of peak-horizontal acceleration to velocity. Individual marks indicate different ground conditions at the observation site. Ratio predicted by the empirical attenuation relations of equations (1) and (2) is indicated by a solid line.

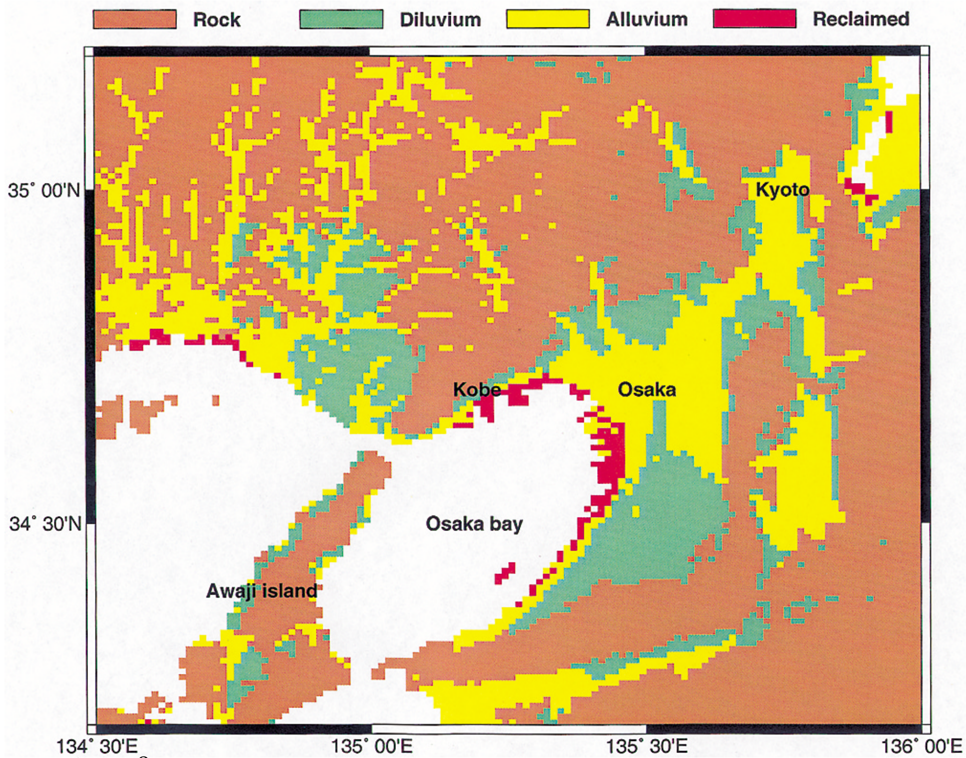

Figure 9. Distribution of classified geological conditions into bedrock, diluvium, alluvium, and reclaimed ground.

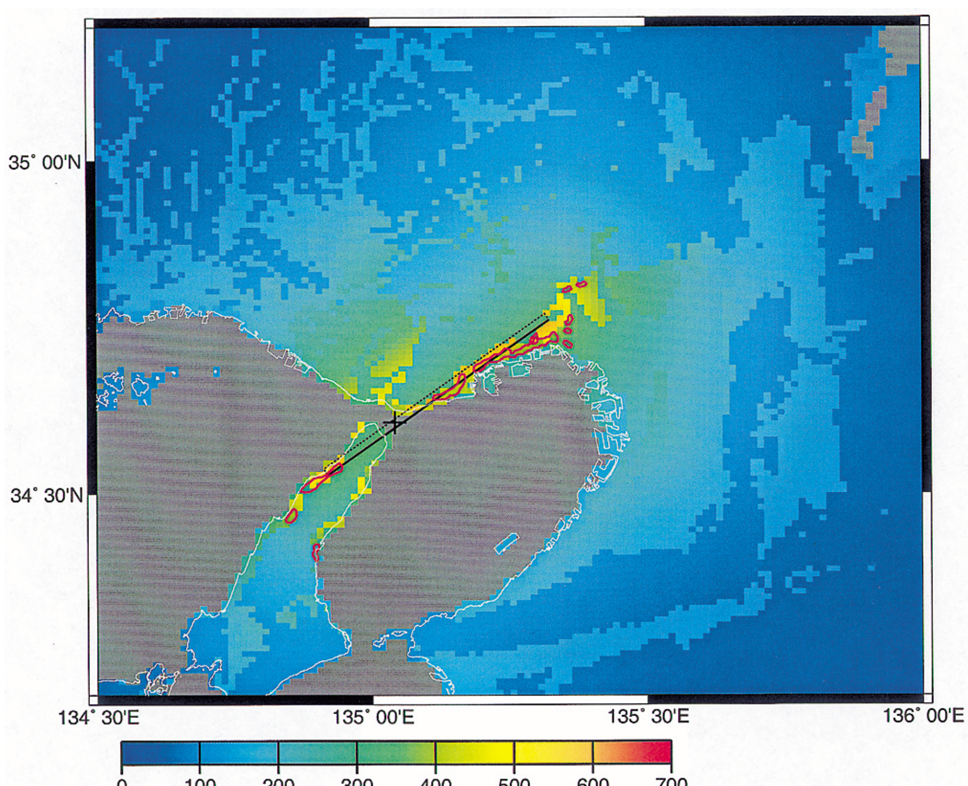

Figure 10. The PHA (cm/sec^2) distribution considering geological correction factors for reclaimed, alluvium, diluvium, and bedrock. Long rectangle indicates assumed fault plane. Cross indicates epicenter. Areas indicated by red line depict the area of JMA intensity VII.

of soils. On the other hand, PVA does not decrease as a result of the nonlinearity, so the ratios of PVA/PVV at short distances are larger than the PHA/PHV ratios, and the ratio of (PVA/PVV)/(PHA/PHV) for reclaimed ground is the largest in Table 2. If a frequency f_0 Hz predominated in the peak amplitude, at a first order approximation, the PHA can be expressed by $2\pi f_0$ PHV. Therefore the mean value of 10 corresponds to the frequency of 1.6 Hz. In the near-fault region, the ratio is about 7 and this corresponds to about 1 Hz, which is consistent with predominant frequencies recorded at many sites near the causative faults. The ratio, which is related to the predominant frequency, for soft soils near the faults tends to further decrease due to the nonlinear behavior. On the contrary, sites of high ratio, for example Higashiyama and Kyoto, belong to areas of forward rupture directivity. Only Gobo is belonging to sideward directivity, but this site is located on thin reclaimed ground over bedrock, and high-frequency phases corresponding to reclaimed layers were predominant. At distances longer than 100 km, the ratio falls off, perhaps due to the contamination caused by the low-frequency surface waves.

Isoseismal Map

The distribution of peak acceleration at the ground surface is very interesting, in particular the characteristics of strong-ground motion at near-fault sites where the number of observations was very limited. On the basis of the findings described in the previous section, we consider that equation (1) represents the average value of the PHA. We used GIS data on a fine grid points with the longitudinal and latitudinal interval of 0.0125 and 0.0083 degree around this area. The ground condition distribution is shown in Figure 9. This also includes the newly reclaimed area. The correction factors are estimated using equations (5) and (6) for the reclaimed and alluvial soil, and multiplying the average value by 55% and 94% for the bedrock and diluvium (Table 2). The surface PHA distribution was estimated by multiplying the predicted value of equation (1) and the correction factors for the completed distribution. In Figure 10, the estimated PHA is compared with the region of JMA intensity VII. Around the east end of the assumed fault plane, the area of the JMA intensity VII is located relatively south of the large PHA area. This divergence might be due to the basin edge effect that probably amplified the ground motion at sites along the basin edge, south of the fault (Kawase, 1996; Pitarka *et al.,* 1998). However in general, the severe damage belt of the JMA intensity VII corresponds to the estimated high amplitude zone.

Conclusions

1. The 1995 Kobe earthquake caused severe structural damage in a modern metropolitan area. However, the observed peak amplitudes agree well with amplitudes predicted by the empirical attenuation equations developed for Japanese earthquakes (Fukushima and Tanaka, 1992; Midorikawa, 1993), suggesting that on average the peak amplitude of the ground motion generated by the damaging earthquake did not exceed the level predicted by the empirical attenuation equation.
2. The ratio of the observed/predicted peak amplitudes for the average horizontal component significantly depends on the local ground conditions. The ratio is larger for soft soils, except for PHA at short distances, where the PHA decreases due to nonlinear behavior of soils. The residual between the observed and predicted PHA is considerably reduced if corrections for the site effect are applied.
3. The ratios of the PVA to PHA for soft soils are greater than 1.0 when PHA decreases as a result of the nonlinear behavior of soils. On the other hand, all of the PVV/PHV are less than 1.0, and are 0.4 on average.
4. The ratio of the PHA to PHV has a peak at around 50 km. This demonstrates that the saturation of the PHA with decreasing distance in the near-source region is more notable than that of the PHV, in particular for soft soils.
5. The average correction factors for the individual geological conditions were derived from the ratio of the observed/predicted PHA. Multiplying the predicted PHA values by the attenuation relation and the correction factors, the PHA distribution reflecting also the effect of the surface geology can be derived for the near-fault region. The estimated high PHA area agrees well with the severe damage belt of the JMA intensity VII.

Acknowledgments

We wish to express our gratitude to all organizations that announced peak amplitudes and made observations available. Most kindly made their sites available to us. We also wish to express gratitude to Dr. Motofumi Watanabe of Shimizu Corp. for his suggestions in the writing of this manuscript and to Dr. Toshio Yamashita of TEPCO for his help in this research project. This manuscript was much improved by the rewriting of Dr. Arben Pitarka of URS Greiner Woodward Clyde Federal Services.

References

Architectural Institute of Japan (1996). 1995nen Hyogoken-Nanbu Jishin Kyoushin Kiroku Shiryousyu, January 1996, Special Working Group for Hyogoken-Nanbu Jishin, AIJ (in Japanese).

Borcherdt, R., and T. Holzer (1996). The January 17, 1995 Hyogoken-Nanbu (Kobe) earthquake, performance of structures, lifelines, and fire protection systems, in *Seismology, Geology, and Geotechnical Issues,* Natl. Inst. Stand. Technol. Spec. Publ. 901, (Editor), R. Chung.

Eriji, J., S. Sawada, Y. Goto, and K. Toki (1996). Peak ground motion characteristics, *Special Issue of Soils and Foundations, Japanese Geotechnical Soc.,* 7–13.

Fukushima, Y., and T. Tanaka (1990). A new attenuation relation for peak horizontal acceleration of strong earthquake ground motion in Japan, *Bull. Seism. Soc. Am.* **80,** 757–783.

Fukushima, Y., and T. Tanaka (1992). Revised attenuation relation of peak horizontal acceleration by using a new data base, *Programme and Abstracts of the Seism. Soc. Japan,* No. 2, 116 (in Japanese).

Fukushima, Y. (1996). Scaling relations for strong ground motion prediction models with M^2 terms, *Bull. Seism. Soc. Am.* **86,** 329–336.

Fukushima, Y. (1997). Comment on "Ground motion attenuation relations for subduction zones," *Seism. Res. Lett.* **68,** 947–949.

Fukushima, Y., T. Watanabe, T. Uetake, and H. Matsumoto (1997). Attenuation characteristics of observed peak amplitude from 1995 Hyogoken Nanbu event, *14th SMiRT* **K02/5,** 83–90.

Fukushima, Y., and K. Irikura (1997). Attenuation characteristics of peak ground motions in the 1995 Hyogo-ken Nanbu earthquake, *J. Phys. Earth* **45,** 135–146.

Fukushima, Y., T. Watanabe, T. Uetake, and H. Matsumoto (1998). Characteristics of peak amplitude for strong ground motion from 1995 Hyogoken nanbu earthquake, in *Proc of the 2nd International Symposium on the Effects of Surface Geology on Seismic Motion,* 1155–1162.

Geo-Research Institute, Osaka (1995). *Heisei 7-nen Hyogoken Nanbu Jishin Sokuhou,* February, 1995 (in Japanese).

Irikura, K., and Y. Fukushima (1995). Attenuation characteristics of peak amplitude in the Hyogoken-Nambu earthquake, *J. Natural Disaster Sciences,* **16,**(3), 39–46.

Japan Society for Earthquake Engineering Promotion (1998). *Strong Motion Array Observation* No. 3 (in Japanese).

Kamae, K., K. Irikura, and A. Pitarka (1998). A technique for simulating strong ground motion using hybrid Green's function, *Bull. Seism. Soc. Am.* **88,** 357–367.

Kamae, K., and K. Irikura (1998). Source model of the 1995 Hyogo-ken Nanbu earthquake and simulation of near-source ground motion, *Bull. Seism. Soc. Am.* **88,** 400–412.

Kashima, T., and Y. Kitagawa (1995). The 1995 Hyogo-ken-nanbu Earthquake, *Prompt Report on Strong Motion Records,* **4,** Building Res. Inst., Ministry of Construction, Japan (in Japanese).

Kawase, H., T. Satoh, K. Fukutake, and K. Irikura (1995). Borehole records observed at the Port Island in Kobe during the Hyogo-ken Nanbu earthquake of 1995 and its simulation, *J. Struct. Constr. Eng., AIJ,* No. 475, 83–92 (in Japanese).

Kawase, H. (1996). The cause of the damage belt in Kobe: "the basin-edge effect", constructive interference of the direct *S*-wave with the basin-induced diffracted/Rayleigh wave, *Seism. Res. Lett.* **67,** 25–34.

Kikuchi, M. (1995). Teleseismic analysis of the Southern Hyogo (Kobe), Japan, earthquake of January 17, 1995, *Yokohama City Univ. Seismological Note* 38.

Matsumoto, H., T. Uetake, Y. Fukushima, and T. Watanabe (1998). Site effect for the attenuation characteristics of observed peak amplitude from 1995 Hyogo-ken Nanbu event, *Proc. of the 10th Japan Earthquake Engineering Symposium* **1,** 541–546 (in Japanese).

Midorikawa, S. (1993). Preliminary analysis for attenuation of peak ground velocity on stiff site, *Proc. of the International Workshop on Strong Motion Data,* **2,** 39–48.

Midorikawa, S., H. Si, and M. Matsuoka (1996). Empirical analysis of peak horizontal velocity for the Hyogo-ken Nanbu, Japan earthquake of January 17, 1995, *Proc. of the 11th World Conference on Earthquake Engineering* 1564, disk 3 of 4.

Miyata, M., Y. Satho, and S. Iai (1995). Mechanism of damage to port facilities during 1995 Hyogo-ken Nanbu earthquake (Part 1)—strong-motion earthquake records in port areas, *Technical Note, The Port and Harbour Research Institute, Ministry of Transport, Japan, 813* (in Japanese).

Mohammadioun, B., and A. Pecker (1984). Low-frequency transfer of seismic energy by superficial soil deposits and soft rocks, *Earthquake Eng. Struct. Dyn.* **12,** 537–564.

Nakamura, Y., K. Hidaka, J. Saita, and S. Sato (1995). Strong accelerations and damage of the 1995 Hyogoken-Nanbu earthquake, *JR Earthquake Information No. 23b,* Railway Technical Research Institute.

Nakamura, Y., F. Uehan, and H. Inoue (1996). Waveform and its analysis of the 1995 Hyogo-Ken-Nanbu earthquake (II), *JR Earthquake Information No. 23d,* Railway Technical Research Institute (in Japanese).

Nakata, T., K. Yomogida, J. Odaka, T. Sakamoto, K. Asahi, and N. Chida (1995). Surface fault ruptures associated with the 1995 Hyogoken-Nanbu earthquake, *J. Geography* **104,** 127–142.

Nakazawa, M., T. Uetake, H. Inada, T. Watanabe, and Y. Fukushima (1998). Relation between peak amplitude and response spectrum of strong ground motion from Hyogo-ken Nanbu earthquake, *Summaries of Technical Papers of the Annual Meeting of the Architectural Institute of Japan B-2,* 129–130 (in Japanese).

National Research Institute for Earth Science and Disaster Prevention, Science and Technology Agency (1995). *Prompt Report on Strong-Motion Accelerograms* No. 46, January 17, 1995, Southern Hyogo Prefecture, Japan (in Japanese).

Pitarka, A., K. Irikura, T. Iwata, and H. Sekiguchi (1998). Three-dimensional simulation of the near-fault ground motion for the 1995 Hyogo-ken Nanbu (Kobe), Japan, earthquake, *Bull. Seism. Soc. Am.* **88,** 428–440.

Public Works Research Institute (1995). Strong-motion acceleration records from public works in Japan (No. 21), *Technical Note of Public Works Research Institute, Ministry of Construction, Japan,* **64.**

Sekiguchi, H., K. Irikura, T. Iwata, Y. Kakehi, and M. Hoshiba (1996). Minute locating of faulting beneath Kobe and waveform inversion of the source process during the 1995 Hyogo-ken Nanbu, Japan, earthquake using strong ground motion records, *J. Phys. Earth* **44,** 473–448.

Sekiguchi, H., K. Irikura, and T. Iwata (2000). Fault Geometry at the 1995 Hyogo-ken Nanbu earthquake, *Bull. Seism. Soc. Am.* **90,** 117–133.

Shimamoto, T. (1995). Mystery of "damage belt" during Kobe earthquake, *Iwanami-Kagaku* **65,** No. 4, 195–198 (in Japanese).

Somerville, P. G., N. F. Smith, R. W. Graves, and N. A. Abrahamson (1997). Modification of empirical strong ground motion attenuation relations to include the amplitude and duration effects of rupture directivity, *Seism. Res. Lett.* **68,** 199–222.

Stewart, J. P., J. D. Bray, R. G. Seed, and N. Sitar (1994). Preliminary report on the principal geotechnical aspects of the January 17, 1994, Northridge earthquake, Earthquake Engineering Research Center Report No. UCB/EERC 94/08, University of California, Berkeley.

Ohsaki Research Institute
Fukoku-seimei BLDG 27F
2-2-2, Uchisaiwai-cho
Chiyoda-ku, 1000011, Tokyo
Japan
yf@ori.shimz.co.jp
(Y. F.)

Disaster Prevention Research Institute
Kyoto University
Gokasho, Uji, 6110011
Japan
(K. I.)

Power Eng. R&D Center
Tokyo Electric Power Company
4-1 Egasaki-cho, Tsurumi-ku
Yokohama, 2308510
Japan
(T. U., H. M.)

Manuscript received 24 May 1999.

Appendix

List of Strong Motion Observation Sites of Kobe Earthquake

No.	Site	Organization	Long. d, m, s(E)	Lat. d, m, s(N)	Level*	Acc/Vel	H1 (cm/sec/sec)	H2 (cm/sec/sec)	UD (cm/sec/sec)	H1 (cm/sec)	H2 (cm/sec)	UD (cm/sec)	H1 comp.†	H2 comp.
1	Takatori	JR	135 08 11	34 38 53	GL	Acc	606	657	279	127.0	127.0	17.3	NS	EW
2	Shin-Kobe	JR	135 11 49	34 42 08	GL	Acc	530	267	344				NS	EW
3	Takarazuka	JR	135 20 37	34 48 37	GL	Acc	684	601	418	71.9	81.5	33.7	NS	EW
4	Nishi-Akashi	JR	134 57 50	34 39 50	GL	Acc	474	455	380	46.8	40.2	21.4	NS	EW
5	Shin-Osaka	JR	135 30 01	34 43 43	GL	Acc	181	216	176	41.0	36.3	11.3	NS	EW
6	Shin-Osaka Trans	JR	135 30 58	34 44 49	GL	Acc	221	229	62	34.3	25.2	6.3	NS	EW
7	Kakogawa	JR	134 50 35	34 45 50	GL	Acc	235	318	168	21.4	27.2	10.2	NS	EW
8	Kankuu Trans	JR	135 15 34	34 26 17	GL	Acc	167	141	122	19.6	23.2	10.7	NS	EW
9	Higashikishiwada	JR	135 23 17	34 26 42	GL	Acc	182	209	79	18.2	12.4	8.0	NS	EW
10	Shin-Takatsuki Trans	JR	135 39 14	34 51 32	GL	Acc	297	231	121				NS	EW
11	Sasayamaguchi	JR	135 10 48	35 03 11	GL	Acc	200	275	57	10.5	13.4	2.8	NS	EW
12	Himeji	JR	134 41 40	34 49 16	GL	Acc	82	125	48				NS	EW
13	Sonobe	JR	135 29 13	35 06 00	GL	Acc	135	254	54	10.8	12.6	5.1	NS	EW
14	Wakayama	JR	135 11 38	34 13 47	GL	Acc	174	126	58	14.4	11.8	5.4	NS	EW
15	Nara	JR	135 49 18	34 40 34	GL	Acc	112	104	36				NS	EW
16	Nijo	JR	135 44 41	35 00 27	GL	Acc	84						max	
17	Higashiyama Trans	JR	135 47 50	34 58 41	GL	Acc	182	209	78	9.5	7.0	3.4	NS	EW
18	Aioi	JR	134 28 29	34 48 54	GL	Acc	62	52	28				NS	EW
19	Hashimato	JR	135 37 02	34 18 54	GL	Acc	21	18	13				NS	EW
20	Tokushima	JR	134 33 04	34 04 19	GL	Acc	82						larger	
21	Fukuchiyama	JR	135 07 16	35 17 35	GL	Acc	108	134	26	4.9	8.3	2.5	NS	EW
22	Ikuno	JR	134 47 52	35 09 36	GL	Acc	36	53	20				NS	EW
23	Iri Trans	JR	134 13 37	34 45 00	GL	Acc	97	77	64				NS	EW
24	Ritto Trans	JR	135 59 45	35 01 41	GL	Acc	60	68	25				NS	EW
25	Gobo	JR	135 09 47	33 54 14	GL	Acc	128	166	39	7.7	10.3	3.6	NS	EW
26	Nishimaizuru	JR	135 19 59	35 26 17	GL	Acc	60	79	20				NS	EW
27	Takamatsu	JR	134 02 55	34 20 49	GL	Acc	94						larger	
28	Tsuge	JR	136 15 32	34 50 35	GL	Acc	77	67	33				NS	EW
29	Gokasyou	JR	136 11 02	35 08 20	GL	Acc	133	140	47	11.1	8.2	4.2	NS	EW
30	Obama	JR	135 44 56	35 29 17	GL	Acc	74	61	26				NS	EW
31	Okayama	JR	133 55 07	34 39 37	1F	Acc	85	58	30				NS	EW
32	Toyooka	JR	134 48 59	35 32 31	GL	Acc	103	90	27				NS	EW
33	Shinjo Trans	JR	133 49 03	34 38 38	GL	Acc	66	46	20				NS	EW
34	Bannosu Trans	JR	133 49 53	34 20 59	GL	Acc	36	24	17				NS	EW
35	Hitsuishi-Jima	JR	133 48 24	34 25 08	GL	Acc	38	17	13				NS	EW
36	Shin-Maibara Trans	JR	136 17 35	35 18 58	GL	Acc	215	138	29	18.7	8.6	2.3	NS	EW
37	Tadotsu	JR	133 45 28	34 15 53	1F	Acc	49						larger	
38	Kii Nagashima	JR	136 20 33	34 12 21	GL	Acc	46						max	
39	Matsuzaka	JR	136 32 18	34 34 26	GL	Acc	49						max	
40	Kazumi	JR	134 37 31	35 38 00	GL	Acc	38	51	21				NS	EW
41	Kinomoto	JR	136 13 26	35 30 18	GL	Acc	50	53	13				NS	EW
42	Awa Ikeda	JR	133 48 25	34 01 24	1F	Acc	35						larger	
43	Tsuruga	JR	136 04 55	35 38 31	GL	Acc	59	41	16				NS	EW
44	Kumanoshi	JR	136 06 09	33 53 11	GL	Acc	52						max	

45	Susami	JR	135 29 54	33 32 34	GL	Acc	23	29	12				NS	EW
46	Yokkaichi	JR	136 37 59	34 57 36	GL	Acc	65						max	
47	Sekigahara	JR	136 28 19	35 21 36	GL	Acc	95						max	
48	Shin-Sekigahara Trans	JR	136 28 56	35 21 29	GL	Acc	106	72	29				NS	EW
49	Shin-Kamogata	JR	133 33 23	34 31 58	GL	Acc	14	16	12				NS	EW
50	Kii Katsuura	JR	135 56 38	33 37 26	GL	Acc	38	38	13				NS	EW
51	Hajima Trans	JR	136 40 20	35 19 34	GL	Acc	58	32	12				NS	EW
52	Osugi	JR	133 40 00	33 45 27	GL	Acc	20						larger	
53	Takefu	JR	136 10 24	35 54 02	GL	Acc	16	19	19				NS	EW
54	Kisogawa	JR	136 47 02	35 20 46	GL	Acc	67						max	
55	Shin-Biwajima Trans	JR	136 52 01	35 11 42	GL	Acc	21	18	7				NS	EW
56	Odaka Trans	JR	136 57 10	35 02 52	GL	Acc	19	14	8				NS	EW
57	Anjo Trans	JR	137 05 56	34 55 44	GL	Acc	22	20	7				NS	EW
58	Fukui	JR	136 13 34	36 03 29	GL	Acc	38	23	18				NS	EW
59	Kochi	JR	133 32 58	33 33 48	GL	Acc	40						larger	
60	Mihara	JR	133 05 06	34 23 51	GL	Acc	30						max	
61	Okazaki	JR	137 09 36	34 55 12	GL	Acc	9						max	
62	Echizen Ono	JR	136 29 57	35 58 46	GL	Acc	20	24	11				NS	EW
63	Mino Ota	JR	137 01 28	35 26 31	GL	Acc	50						max	
64	Shin Mihara Trans	JR	133 02 36	34 23 43	GL	Acc	16	16	7				NS	EW
65	Iyo Saijo	JR	133 11 30	33 54 33	GL	Acc	20						max	
66	Tajimi	JR	137 07 19	35 19 48	GL	Acc	15						max	
67	Otsuka	JR	137 16 48	34 48 40	GL	Acc	10	9	4				NS	EW
68	Toyohashi	JR	137 23 13	34 45 26	GL	Acc	12						max	
69	Miyoshi	JR	132 51 31	34 47 58	GL	Acc	9						max	
70	Daisyouji	JR	136 18 58	36 17 52	GL	Acc	58	63	20				NS	EW
71	Suzaki	JR	133 17 48	33 23 14	GL	Acc	12						larger	
72	Shin-Saijo Trans	JR	132 46 41	34 23 43	GL	Acc	22	14	5				NS	EW
73	Gero	JR	137 14 32	35 48 07	GL	Acc	12						max	
74	Nakatsugawa	JR	137 30 18	35 29 42	GL	Acc	14						max	
75	Mikawa	JR	136 29 35	36 29 02	GL	Acc	40	28	11				NS	EW
76	Kobe	JMA	135 10 46	34 41 18	GL	Acc	818	617	332	91.0	75.0	40.0	NS	EW
77	Osaka	JMA	135 31 18	34 40 42	B3F	Acc	81	66	65	19.4	15.6	7.1	NS	EW
78	Kyoto	JMA	135 44 08	35 00 43	GL	Acc	160	197	36	15.0	11.0	4.7	NS	EW
79	Tokushima	JMA	134 34 36	34 03 53	GL	Acc	94	90	35	12.0	10.0	3.5	NS	EW
80	Maizuru	JMA	135 19 13	35 26 49	GL	Acc	67	52	39	4.6	4.9	2.1	NS	EW
81	Takamatsu	JMA	134 03 26	34 18 53	GL	Acc	68	87	34	6.3	9.8	2.6	NS	EW
82	Okayama	JMA	133 55 08	34 39 27	B1F	Acc	77	59	36	5.3	3.8	2.7	NS	EW
83	Toyooka	JMA	134 49 31	35 31 59	GL	Acc	87	138	50	15.0	10.0	3.5	NS	EW
84	Hikone	JMA	136 14 48	35 16 23	GL	Acc	137	147	39	16.0	15.0	3.1	NS	EW
85	Tsu	JMA	136 31 25	34 43 53	B1F	Acc	71	60	26	6.4	6.7	3.0	NS	EW
86	Tottori	JMA	134 14 28	35 29 06	GL	Acc	77	74	15	9.9	9.2	1.0	NS	EW
87	Shionomisaki	JMA	135 45 50	33 26 52	GL	Acc	19	24	9	1.9	1.6	1.4	NS	EW
88	Gifu	JMA	136 45 56	35 23 49	1F	Acc	32	22	9	3.1	3.4	1.1	NS	EW
89	Nagoya	JMA	136 58 05	35 09 52	GL	Acc	16	14	10	3.3	2.5	0.92	NS	EW
90	Muroto	JMA	134 10 48	33 14 53	GL	Acc	23	13	9	2.2	3.6	1.5	NS	EW
91	Fukui	JMA	136 13 32	36 03 11	GL	Acc	33	42	10	4.0	5.3	1.5	NS	EW
92	Yonago	JMA	133 20 30	35 25 35	GL	Acc	19	21	8	2.5	2.1	0.90	NS	EW

No.	Site	Organization	Long. d, m, s(E)	Lat. d, m, s(N)	Level*	Acc/Vel	H1 (cm/sec/sec)	H2 (cm/sec/sec)	UD (cm/sec/sec)	H1 (cm/sec)	H2 (cm/sec)	UD (cm/sec)	H1 comp.†	H2 comp.
93	Matsuyama	JMA	132 46 50	33 50 24	GL	Acc	14	21	6	2.4	1.2	0.92	NS	EW
94	Kobe Port	PHRI	135 12 31	34 41 10	GL	Acc	502	205	283	100.0	35.0	32.0	N43W	N47E
95	Pier 8	PHRI	135 13 02	34 41 15	pier	Acc	683	394	334	185.0	61.0	38.0	N42W	N48E
96	Amagasaki	PHRI	135 24 14	34 42 43	GL	Acc	321	472	311	52.0	57.0	27.0	N06W	N84E
97	Osaka	PHRI	135 26 40	34 38 46	GL	Acc	178	125	103				S24E	E24N
98	Wakayama	PHRI	135 08 54	34 12 51	GL	Acc	157	109	67				N12E	E12S
99	Komatsujima	PHRI	134 35 17	34 02 50	GL	Acc	89	96	32				NS	EW
100	Tsuruga	PHRI	136 03 55	35 39 14	GL	Acc	56	51	20				NS	EW
101	Yokkaichi	PHRI	136 38 26	34 57 00	GL	Acc	54	41	11				NS	EW
102	Nagoya	PHRI	136 52 06	35 04 22	pier	Acc	30	32	12				S20W	E20S
103	Kinuura	PHRI	136 56 48	34 52 41	GL	Acc	27	25	9				NS	EW
104	Kochi	PHRI	133 34 10	33 30 18	GL	Acc	28	26	10				NS	EW
105	Sakaiminato	PHRI	133 15 04	35 32 32	GL	Acc	44	33	16				NS	EW
106	Matsuyama	PHRI	132 42 52	33 51 17	GL	Acc	40	35	10				NS	EW
107	Amagasaki Bridge	PWRI	135 25 20	34 42 35	GL	Acc	265	294	324	52.0	51.0	23.0	N150E	N240E
108	Oyodo	PWRI	135 29 11	34 42 18	GL	Acc	203	221	239	34.0	31.0	8.2	N68E	N158E
109	Yodogawa EMB.	PWRI	135 31 13	34 42 54	GL	Acc	138	119	101	16.0	14.0	5.3	LG	TR
110	Kakogawa	PWRI	134 53 30	34 47 30	bank	Acc	144	211	264				LG	TR
111	Hirakata	PWRI	135 38 50	34 48 52	GL	Acc	293	397	140	17.0	20.0	5.1	N45E	N135E
112	Yamatogawa	PWRI	135 35 32	34 35 19	GL	Acc	156	199	56	8.9	17.0	5.2	EW	NS
113	Kinokawa	PWRI	135 09 12	34 13 32	GL	Acc	129	105	65	22.0	14.0	5.4	N62E	N152E
114	Kinokawa Bridge	PWRI	135 09 59	34 12 50	GL	Acc	106	145	52	13.0	9.5	4.8	N120E	N210E
115	Amagase	PWRI	135 49 49	34 52 36	tunnel	Acc	107	56	28	5.9	3.0	2.4	LG	TR
116	Tokushima	PWRI	134 33 27	34 05 11	GL	Acc	133	119	50	14.0	8.9	4.5	LG	TR
117	Ishii	PWRI	134 27 17	34 05 54	GL	Acc	119	91	97	10.0	8.8	6.7	LG	TR
118	Sarutani Dam	PWRI	135 44 42	34 10 35	GL	Acc	39	18	12	1.9	1.4	1.2	EW	NS
119	Minato Bridge	PWRI	134 49 41	35 38 25	GL	Acc	73	66	39	6.6	7.8	4.1	N130E	N220E
120	Akagi Bridge	PWRI	135 51 15	33 46 24	GL	Acc	60	43	9					
121	Higashi Kobe Bridge	PWRI	135 17 45	34 42 24	GL	Acc	281	327	395	82.0	87.0	36.0	N78E	N168E
122	Inagawa	PWRI	135 25 37	34 49 44	GL	Acc	422	417	361	40.0	40.0	20.0	NS	EW
123	Yotsubashi	PWRI	135 30 00	34 40 08	GL	Acc	252	330	223	29.0	21.0	8.4	NS	EW
124	Matsunohama p32	PWRI	135 24 24	34 30 23	GL	Acc	145	135	116	15.0	13.0	4.7	N59E	N149E
125	Matsunohama p23	PWRI	135 24 39	34 30 31	GL	Acc	169	107	106	20.0	9.8	4.5	N59E	N149E
126	Suita Shimizu	PWRI	135 32 47	34 48 04	1F	Acc	485							
127	Naruto	Hon-Shi B.A.	134 39 49	34 14 15	tunnel	Acc	136	119	48	16.0	13.0	4.0	TR	LG
128	Kobe Univ.	CEORKA	135 14 26	34 43 30	tunnel	Vel	305	270		51.0	31.0	33.2	NS	EW
129	Fukushima	CEORKA	135 28 26	34 41 13	1F	Vel	180	212	195	30.9	29.8	9.6	NS	EW
130	Abeno	CEORKA	135 31 08	34 38 10	GL	Vel	217	226	136	21.3	24.9	6.3	NS	EW
131	Morikawachi	CEORKA	135 34 19	34 40 48	1F	Vel	210	123	159	27.1	24.7	6.1	NS	EW
132	Sakai	CEORKA	135 28 08	34 33 50	1F	Vel	150	125	100	15.9	15.7	6.6	NS	EW
133	Yae	CEORKA	135 36 43	34 40 48	1F	Vel	155	145	127	21.2	21.8	7.0	NS	EW
134	Tadaoka	CEORKA	135 24 29	34 28 48	1F	Vel	290	190	137	24.4	14.7	6.9	NS	EW
135	Chihaya	CEORKA	135 37 32	34 26 20	base	Vel	91	109	74	5.2	4.9	2.4	NS	EW
136	Fukiai	Ohsaka Gas	135 12 39	34 41 42	GL	Acc	687	802		58.0	123.0		N120W	N030W
137	Nishinomiya	Ohsaka Gas	135 21 04	34 43 17	GL	Vel	792						max	
138	Hokkou	Ohsaka Gas	135 25 47	34 40 03	GL	Vel	266						max	
139	Iwasaki	Ohsaka Gas	135 28 50	34 39 55	GL	Vel	169	139		24.0	19.0		NS	EW

140	Senri	Ohsaka Gas	135 31 13	34 48 15	GL	Acc	299	185		28.0	17.0		N20E	N110E
141	Sakai	Ohsaka Gas	135 26 53	34 36 05	1F	Vel	173			32.0			max	
142	Senpoku2	Ohsaka Gas	135 24 30	34 32 26	1F	Vel	240						max	
143	Hashiramoto	Ohsaka Gas	135 36 10	34 46 57	GL	Vel	251			31.0			max	
144	Kawachi	Ohsaka Gas	135 35 36	34 41 32	GL	Vel	177			34.0			max	
145	Senpoku1	Ohsaka Gas	135 26 16	34 32 26	1F	Acc	178						max	
146	Shijounawate	Ohsaka Gas	135 37 55	34 44 21	GL	Acc	221	256		24.0	28.0		N90W	NS
147	Toubushisya	Ohsaka Gas	135 37 12	34 40 05	GL	Vel	180	130		23.0	19.0		NS	EW
148	Himeji	Ohsaka Gas	134 41 52	34 45 39	1F	Vel	189						max	
149	Onji	Ohsaka Gas	135 37 34	34 36 19	1F	Vel	169			22.0			max	
150	Fujidera	Ohsaka Gas	135 36 33	34 33 52	GL	Vel	198	148		12.0	7.1		NS	EW
151	Sayama	Ohsaka Gas	135 32 47	34 29 46	GL	Vel	160	186		9.0	11.0		NS	EW
152	Shikama	Ohsaka Gas	134 40 35	34 47 28	GL	Acc	253						max	
153	Matsue	Ohsaka Gas	135 08 27	34 14 20	GL	Vel	160	157		22.0	20.0		NS	EW
154	Heijou	Ohsaka Gas	135 45 23	34 43 32	GL	Acc	111	140		7.8	9.1		N60E	N150E
155	Nakanoshima	Ohsaka Gas	135 11 01	34 14 04	GL	A & V	107	106		15.0	12.0		NS	EW
156	Fushimi	Ohsaka Gas	135 44 35	34 55 35	GL	A & V	178	152		18.0	7.3		N135W	N45W
157	Kyoto	Ohsaka Gas	135 44 28	34 59 31	GL	Vel	294	145		13.0	9.1		NS	EW
158	Shin-Kobe Trans	KEPCO	135 15 00	34 43 50	GL	Acc	511	584	495	63.0	77.0	26.0	NS	EW
159	Amagasaki	KEPCO	135 23 27	34 41 24	GL	Acc	227	354	373	45.0	50.0	20.0	NS	EW
160	Sougougiken	KEPCO	135 26 30	34 44 35	GL	Acc	299	648	205	37.0	48.0	21.0	NS	EW
161	Nankou	KEPCO	135 24 30	34 36 50	GL	Acc	107	126	199	21.0	20.0	12.0	NS	EW
162	Takasago	KEPCO	134 45 52	34 45 17	GL	Acc	191	198	182	34.0	44.0	12.0	NS	EW
163	Yao	KEPCO	135 36 40	34 36 10	GL	Vel	148	139	82	13.0	13.0	4.8	NS	EW
164	Minami Osaka	KEPCO	135 28 30	34 27 50	GL	Vel	144	145	93	14.0	12.0	3.9	NS	EW
165	Shigi	KEPCO	135 39 07	34 35 46	GL	Acc	42	46	28	3.4	2.9	0.94	NS	EW
166	Nishi-Kyoto	KEPCO	135 37 20	34 58 00	GL	Acc	114	129	83	14.0	11.0	6.2	NS	EW
167	Kainan	KEPCO	135 11 22	34 09 04	GL	Acc	98	128	92	8.4	9.4	3.7	NS	EW
168	Akou	KEPCO	134 22 45	34 44 05	GL	Acc	104	84	122	11.0	11.0	3.8	N50E	N140E
169	Yamazaki	KEPCO	134 36 10	35 03 35	GL	Acc	131	92		3.6	4.8		NS	EW
170	Gobo	KEPCO	135 09 10	33 51 22	GL	Acc	60	74	26	2.4	3.7	0.94	N12W	N78E
171	Takahama	KEPCO	135 30 30	35 31 10	base	Acc	17	23	16				N140W	N050W
172	Miyazu	KEPCO	135 15 20	35 33 15	GL	Acc	57	70	57	3.2	4.1	1.7	N030E	N120E
173	Oi	KEPCO	135 39 17	35 32 15	base	Acc	12	12	13				N040W	N050E
174	Yuzaki	KEPCO	135 21 12	33 40 24	GL	Vel	16	19	8	2.3	2.9	1.3	NS	EW
175	Mihama	KEPCO	135 57 47	35 42 04	base	Acc	16	14	6				N105W	N015W
176	Ousakayama	Shiga Pref.	135 51 40	34 59 53	tunnel	Vel	45	43	40	6.6	4.0	3.5	NS	EW
177	Kusatsu	Shiga Pref.	135 57 29	35 00 40	GL	Vel	145	89	37	11.5	7.8	4.9	NS	EW
178	Kuzugawa	Shiga Pref.	135 51 04	35 13 32	GL	Vel	29	37	20	6.2	4.0	2.8	NS	EW
179	Minaguchi	Shiga Pref.	136 10 12	34 58 05	GL	Vel	43	41	23	4.1	3.0	2.5	NS	EW
180	Imazu	Shiga Pref.	136 02 06	35 24 11	GL	Vel	47	43	22	4.2	3.9	2.0	NS	EW
181	Torahime	Shiga Pref.	136 15 54	35 24 58	GL	Vel	70	65	21	6.9	6.4	2.1	NS	EW
182	Shiga Tandai	Shiga Pref. J. College	136 13 41	35 15 33	GL	Acc	78	28	24	10.0	5.0	2.6	NS	EW
183	Abuyama	RCEP, Kyoto Univ.	135 34 25	34 51 36	tunnel	Vel	78	81	57	10.0	9.1	7.6	NS	EW
184	Wachi	RCEP, Kyoto Univ.	135 24 05	35 16 57	tunnel	Vel	18	21	17	2.4	3.2	2.9	NS	EW

No.	Site	Organization	Long. d, m, s(E)	Lat. d, m, s(N)	Level*	Acc/Vel	H1 (cm/sec/sec)	H2 (cm/sec/sec)	UD (cm/sec/sec)	H1 (cm/sec)	H2 (cm/sec)	UD (cm/sec)	H1 comp.†	H2 comp.
185	Oya	RCEP, Kyoto Univ.	134 39 57	35 19 18	tunnel	Vel	38	25	25	3.9	3.2	2.4	NS	EW
186	Kume	RCEP, Kyoto Univ.	133 50 57	35 05 19	tunnel	Vel	14	13	13	3.2	1.5	1.0	NS	EW
187	Azai	RCEP, Kyoto Univ.	136 19 10	35 28 38	GL	Vel	25	23	11	2.6	2.1	1.1	NS	EW
188	Res. Reactor	RRI, Kyoto Univ.	135 20 58	34 22 58	base	Acc	218	166	151					
189	DPRI Osaka JMA	DPRI, Kyoto Univ.	135 32 13	34 40 41	B2F	Acc	81	68	79					
190	N	Ohsaka Inst. Tech.	135 25 43	34 37 54	GL	Acc	76	77					NS	EW
191	D	Ohsaka Inst. Tech.	135 32 45	34 43 39	GL	Acc	189	155	126				NS	EW
192	A	Ohsaka Inst. Tech.	135 30 50	34 38 31	GL	Acc	76		26				NS	EW
193	P	Ohsaka Inst. Tech.	135 38 04	34 39 00	GL	Acc	152	145	101				NS	EW
194	U	Ohsaka Inst. Tech.	135 39 15	34 39 06	GL	Acc	110	104	55				NS	EW
195	RA	Ohsaka Inst. Tech.	135 21 34	34 22 42	GL	Acc	57		56				NS	EW
196	H	Ohsaka Inst. Tech.	135 47 56	34 35 30	GL	Acc	108	104	44				NS	EW
197	Kansai Univ.	Kansal Univ.	135 34 47	34 52 27	GL	Acc	67	61	36	9.4	8.2	4.9	NS	EW
198	Osaka	BRI	135 31 08	34 41 17	B3F	Acc	90	83	109					
199	Maizuru	BRI	135 23 20	35 28 23	1F	Acc	85	70	19					
200	Matsuzaka	BRI	136 36 58	34 36 36	1F	Acc	70	64	34					
201	Yonago	BRI	133 19 59	35 25 37	B1F	Acc	26	22	7					
202	Banpaku	NTT	135 31 54	34 48 05	1F	Acc	266	125	103					
203	Himeji	NTT	134 41 52	34 49 45	1F	Acc	88	50	38					
204	Komatsu	NTT	136 26 50	36 23 44	1F	Acc	38	22	6					
205	Obayashi Bldg.	Obayashi	135 30 07	34 41 20	B2F	Acc	139	87	210	21.2	21.2	9.2	SN	WE
206	Taisho	Obayashi	135 28 42	34 38 59	GL	Vel	202	155	168	27.6	26.6	11.1	NS	EW
207	M	Obayashi	135 31 21	34 42 14	B2F	Acc	60	86	42	14.6	13.1	7.4	SN	WE
208	Abiko	Obayashi	135 30 06	34 35 51	1F	Vel	108	115	113	16.7	13.6	7.9	NS	EW
209	B	Takenaka	135 30 17	34 42 10	GL	Acc	182	267	302	23.0	2.9	10.0	N140E	N130E
210	Y	Takenaka	135 31 09	34 41 51	GL	Acc	43	50	49	4.3	7.7	2.1	NS	EW
211	T	Takenaka	135 34 55	34 30 47	GL	Acc	53	50	46				NS	EW
212	Rokkou	Hankyu RW	135 14 15	34 42 59	1F	Acc	499						max	
213	Nakatsu	Hankyu RW	135 29 35	34 42 25	GL	Acc	206						max	
214	Saiin	Hankyu RW	135 43 52	34 59 52	GL	Acc	199						max	
215	Kitashiro	Hanshin RW	135 25 19	34 42 51	1F	Acc	303						max	
216	Tanigami	Hokushin RW	135 10 25	34 45 32	1F	Acc	356						max	
217	Hirano	Nose RW	135 25 09	34 51 54	1F	Acc	276							
218	Port Island	Kobe City	135 12 29	34 40 11	GL	Acc	341	284	556	85.0	51.0	63.0	NS	EW
219	Matsumura RI	Matsumura gumi	135 13 00	34 51 21	GL	Acc	268	265	239	23.0	35.0	9.2	N334E	N064E
220	WEST	Ministry Post Tel.	135 13 06	34 51 36	GL	Acc	263	300	213	25.0	36.0	13.0	NS	EW
221	Takami	Juto Koudan	135 27 43	34 41 25	GL	Acc	222	267	255	31.0	33.0	11.0	NS	EW
222	Kansai Airport	Kansai Airport	135 15 21	34 26 15	GL	Vel	169	104	247	18.0	23.0	8.3	N57E	N147E
223	NHK Kobe	NHK	135 11 28	34 41 29	1F	Acc	680	368					NS	EW

No.	Distance (km)	Situation	Instrument	Period Range	Wave	Saturate	Boring	PS log	Geology	Topography	Reference
1	0.6	noise interference	SM-10A	0.1–	○		○		alluvium	flat	JR, Earthq. Info., 23d
2	1.4	next to tunnel	NEWS-II		○				diluvium	cliff	JR, Earthq. Info., 23d
3	5.9	noise interference in EW	SM-10A	0.1–	○	EW	○		diluvium	gentle slope	JR, Earthq. Info., 23d
4	10.0	under elevated RW	NEWS-II	0.1–	○		○		diluvium	flat	JR, Earthq. Info., 23d
5	16.7	next to elevated RW	SM-10A	0.1–	○		○		alluvium	flat	JR, Earthq. Info., 23d
6	17.8		NEWS-II	0.1–	○		○		alluvium	flat	JR, Earthq. Info., 23d
7	25.4		SM-10A	0.1–	○		○		alluvium	flat	JR, Earthq. Info., 23d
8	25.8	Long. & Lat. had error of about 1′	NEWS-R89	0.1–	○				reclaimed	flat	JR, Earthq. Info., 23d
9	32.1	southwest of station	NEWS-R84	0.1–	○		○		diluvium	flat	JR, Earthq. Info., 23d
10	32.3		NEWS-II						alluvium	flat	JR, Earthq. Info., 23d
11	34.9	on platform	NEWS-R84	0.1–	○				diluvium	flat	JR, Earthq. Info., 23d
12	38.4	under elevated RW	NEWS-II				○		alluvium	flat	JR, Earthq. Info., 23d
13	40.5		NEWS-R84	0.1–	○				diluvium	flat	JR, Earthq. Info., 23d
14	42.3	north end of station	NEWS-R89	0.1–	○		○		alluvium	flat	JR, Earthq. Info., 23d
15	46.7	southeast end of station	NEWS-R84				○		alluvium	flat	JR, Earthq. Info., 23d
16	47.4		NEWS-R89				○		alluvium	flat	JR, Earthq. Info., 23d
17	49.7	next to tunnel	NEWS-II	0.1–	○		○		diluvium	mountain skirts	JR, Earthq. Info., 23d
18	51.6	under elevated RW	NEWS-II				○		alluvium	gentle slope	JR, Earthq. Info., 23d
19	56.1	west of station	NEWS-R84				○		bedrock	flat	Prompt Report 46, NIED
20	60.9	removed	HGA-2B				○		bedrock	flat	JR, Earthq. Info., 23d
21	61.7	next to station building	NEWS-R84	0.1–	○		○		alluvium	flat	JR, Earthq. Info., 23d
22	63.6	unknown	NEWS-R84						BR or AL	flat	JR, Earthq. Info., 23d
23	67.9		NEWS-II						alluvium	flat mountain skirts	JR, Earthq. Info., 23d
24	68.4		NEWS-II	0.2–			○		alluvium	flat	JR, Earthq. Info., 23d
25	72.7	southeast of station	NEWS-R89	0.1–	○		○		BR or AL	flat	JR, Earthq. Info., 23d
26	75.0	next to Kitatango RW station	NEWS-R84				○		alluvium	flat	JR, Earthq. Info., 23d
27	82.5	removed	HGA-2B				○		reclaimed	flat	JR, Earthq. Info., 23d
28	86.3	center of station	NEWS-R84						diluvium	gentle slope	JR, Earthq. Info., 23d
29	89.2		NEWS-II	0.1–	○				alluvium	flat but near mountain	JR, Earthq. Info., 23d
30	89.5		NEWS-R84	0.2–			○		alluvium	flat	JR, Earthq. Info., 23d
31	92.8	under elevated RW	NEWS-II				○	○	alluvium	flat	JR, Earthq. Info., 23d
32	97.9		NEWS-R84				○		alluvium	flat	JR, Earthq. Info., 23d
33	101.7		NEWS-II						alluvium	flat	JR, Earthq. Info., 23d
34	101.9	next to bridge pier	NEWS-II						reclaimed	flat	JR, Earthq. Info., 23d
35	102.9		NEWS-II						bedrock	slope	JR, Earthq. Info., 23d
36	107.9	unknown	NEWS-II	0.1–	○				alluvium	flat	JR, Earthq. Info., 23d
37	110.7	under stairs	SMAC-B2				○		alluvium	flat	JR, Earthq. Info., 23d
38	112.2	northwest on the platform	NEWS-R84						alluvium	flat	JR, Earthq. Info., 23d
39	113.5	north of station	NEWS-R84				○		alluvium	flat	JR, Earthq. Info., 23d
40	115.4		NEWS-R84						alluvium	flat	JR, Earthq. Info., 23d
41	116.5		NEWS-R84						alluvium	flat	JR, Earthq. Info., 23d
42	116.8	1F of 2-story building	SMAC-B2						diluvium	flat	JR, Earthq. Info., 23d
43	119.7	Long. had error of about 3′.	NEWS-R84	0.2–			○		alluvium	flat	JR, Earthq. Info., 23d
44	120.7	under bridge	NEWS-R84						BR or AL	flat	JR, Earthq. Info., 23d

No.	Distance (km)	Situation	Instrument	Period Range	Wave	Saturate	Boring	PS log	Geology	Topography	Reference
45	121.5	west of station	NEWS-R89				○		bedrock	flat	JR, Earthq. Info., 23d
46	122.0	under bridge	NEWS-R84				○		alluvium	flat	JR, Earthq. Info., 23d
47	124.2		NEWS-R84						alluvium	flat	JR, Earthq. Info., 23d
48	124.9		NEWS-II						Neogene	flat mountain skirts	JR, Earthq. Info., 23d
49	125.0		NEWS-II						alluvium	gentle slope	JR, Earthq. Info., 23d
50	136.0	southeast of station	NEWS-R89				○		Neogene	flat	JR, Earthq. Info., 23d
51	138.3		NEWS-II	0.2–					alluvium	flat, bank	JR, Earthq. Info., 23d
52	143.8		SMAC-B2						bedrock	steep slope	JR, Earthq. Infol., 23d
53	148.2	next to platform	NEWS-R84	0.2–			○		alluvium	flat	JR, Earthq. Info., 23d
54	148.4	center of station	NEWS-R84				○		alluvium	flat	JR, Earthq. Info., 23d
55	149.1		NEWS-II				○		alluvium	flat	JR, Earthq. Info., 23d
56	152.5		NEWS-II	0.2–					Neogene	flat	JR, Earthq. Info., 23d
57	163.7	on bank	NEWS-II	0.2–					diluvium	flat	JR, Earthq. Info., 23d
58	165.6	north of station	NEWS-R84	0.2–			○		alluvium	flat	JR, Earthq. Info., 23d
59	165.7	northeast of station	SMAC-B2				○		alluvium	flat	JR, Earthq. Info., 23d
60	168.9	under elevated RW	HGA-2				○		alluvium	flat	JR, Earthq. Info., 23d
61	169.1	southeast next to RW	NEWS-R84				○		diluvium	flat	JR, Earthq. Info., 23d
62	172.3	next to station building	NEWS-R84	0.2–			○		alluvium	flat	JR, Earthq. Info., 23d
63	172.7	next to building	SM-10A				○		diluvium	flat	JR, Earth. Info., 23d
64	172.8		NEWS-II						BR or AL	valley	JR, Earthq. Info., 23d
65	173.4	200 m west of station	HGA-2B						alluvium	flat	JR, Earthq. Info., 23d
66	176.0	south of station	NEWS-R84						alluvium	flat	JR, Earthq. Info., 23d
67	179.4		NEWS II	0.2–					diluvium	flat	JR, Earthq. Info., 23d
68	189.2	southeast end	NEWS-R84						diluvium	flat	JR, Earthq. Info., 23d
69	190.8	east of station	HGA-2				○		Neogene	flat	JR, Earthq. Info., 23d
70	192.7	on platform	NEWS-R84	0.2–			○		alluvium	flat	JR, Earthq. Info., 23d
71	196.3		SMAC-B2				○		alluvium	flat	JR, Earthq. Info., 23d
72	197.0	next to tunnel	NEWS-II						bedrock	flat	JR, Earthq. Info., 23d
73	209.4	northwest end	NEWS-R84						diluvium	on support wall of 5 m	JR, Earthq. Info., 23d
74	215.1	center of station	NEWS-R84						alluvium	flat	JR, Earthq. Info., 23d
75	218.5	next to platform	NEWS-R84	0.2–			○		alluvium	flat	JR, Earthq. Info., 23d
76	1.0	on small sensor table	JMA87	0.02–10	○		○		diluvium	on small hill	
77	20.4	on small sensor table, removed	JMA87	0.02–10	○		○			flat	
78	47.0	on small sensor table	KI-03A	0.02–10	○		○		alluvium	flat	
79	60.3	on small sensor table	KI-03A	0.02–10	○		○		reclaimed	flat	
80	76.0	on small sensor table	JMA87	0.02–10	○				reclaimed	flat	
81	82.7	on small sensor table	KI-03A	0.02–10	○				alluvium	flat	
82	92.7	on small sensor table	JMA87	0.02–10	○		○		alluvium	flat	
83	96.6	on small sensor table	KI-03A	0.02–10	○		○		alluvium	flat	
84	101.8	on small sensor table	JMA87	0.02–10	○		○		alluvium	flat	
85	110.1	on small sensor table, B1F of 5-story building	JMA87	0.02–10	○		○		alluvium	flat	
86	122.0	on small sensor table in 3-story building	JMA87	0.02–10	○		○		alluvium	flat	
87	142.8	on small sensor table	JMA87	0.02–10	○		○		bedrock	flat	
88	149.4	moved April 1995	KI-03A	0.02–10	○				diluvium	flat, next to river	
89	156.9	on small sensor table	JMA87	0.02–10	○		○		diluvium	hilltop, flat	
90	157.6	on sensor table through 1 story	JMA87	0.02–10	○		○		bedrock	hilltop	
91	165.1	on small sensor table	JMA87	0.02–10	○		○		alluvium	flat	
92	174.9	on small sensor table	JMA87	0.02–10	○				alluvium	flat	

93	211.4	on small sensor table	JMA87	0.02–10	○		○		alluvium	flat	
94	0.8	hut	SMAC-B2		○		○	○	reclaimed	flat	Tech. Note, 813, PHRI
95	1.1	pier sustained major damage	ERS-G		○		○	○		on pier	Tech. Note, 813, PHRI
96	9.2	hut, under water level	ERS-G		○		○		reclaimed	flat	Tech. Note, 813, PHRI
97	16.9	hut, sensor was changed to ERS	SMAC-B2		○		○		reclaimed	flat	Tech. Note, 813, PHRI
98	40.6	hut	ERS-G		○		○		alluvium	flat	Tech. Note, 813, PHRI
99	61.5	hut, removed	ERS-G		○		○		reclaimed	flat	Tech. Note, 813, PHRI
100	119.9	warehouse	ERS-G		○		○		alluvium	flat	Tech. Note, 813, PHRI
101	122.5	warehouse	SMAC-B2		○		○		alluvium	flat	Tech. Note, 813, PHRI
102	145.5	pier	SMAC-B2		○		○		reclaimed	on pier	Tech. Note, 813, PHRI
103	149.3		SMAC-B2		○		○		reclaimed	flat	Tech. Note, 813, PHRI
104	168.6	hut	ERS-G		○		○		alluvium	flat	Tech. Note, 813, PHRI
105	188.5	hut	ERS-G		○		○		reclaimed	flat	Tech. Note, 813, PHRI
106	216.5	hut	ERS-G		○		○		reclaimed	flat	Tech. Note, 813, PHRI
107	10.8	southwest end of school	SMAC-Q	0.1–3.0	○		○		alluvium	flat	Tech. Note, 64, PWRI
108	16.3		SMAC-Q	0.1–3.0	○				alluvium	flat	Tech. Note, 64, PWRI
109	18.8	few meters from river	SM-10A	0.1–3.0	○		○		diluvium	next to river	Tech. Note, 64, PWRI
110	25.4	in bank	SM-10A	0.1–3.0	○				alluvium	in bank	Tech. Note, 64, PWRI
111	30.4	hut	SMAC-B2	0.1–3.0	○		○		alluvium	flat	Tech. Note, 64, PWRI
112	31.3	hut	SMAC-Q	0.1–3.0	○		○		alluvium	flat	Tech. Note, 64, PWRI
113	39.8	next to bank	SMAC-MD	0.1–3.0	○				alluvium	under bank	Tech. Note, 64, PWRI
114	41.4		SMAC-B2	0.1–3.0	○		○		alluvium	flat	Tech. Note, 64, PWRI
115	48.3	another sensor was installed on a floor of building	SM-10	0.1–3.0	○				bedrock	cliff	Tech. Note, 64, PWRI
116	59.3	hut	SMAC-Q	0.1–3.0	○		○		alluvium	flat	Tech. Note, 64, PWRI
117	64.1	hut	SMAC-Q	0.1–3.0	○		○		alluvium	flat	Tech. Note, 64, PWRI
118	75.4	172,154,59 Gal in prompt report were error.	SM-10A	0.1–3.0	○				bedrock	steep slope	Tech. Note, 64 PWRI
119	107.2	next to river, LG direction 65° 40′	SMAC-B2	0.1–3.0	○				alluvium	flat	Tech. Note, 64 PWRI
120	117.9	removed from Technical Note of PWRI	SMAC-B2						Neogene	gentle slope	Tech. Note, 64, PWRI
121	3.5	bore hole GL-35m, H1:425.4, H2:282.0	SA-355CT	0.03–10	○		○		reclaimed	reclaimed	Tech. Note, 64, PWRI
122	12.2	bore hole GL-30m, NS 200, EW 186, UD 152	SA-355CT	0.03–10	○		○		alluvium	next to river	Tech. Note, 64, PWRI
123	19.2	under overpass	SA-355CT	0.03–10	○		○		alluvium	flat	Tech. Note, 64, PWRI
124	27.5	under overpass, next to bank, long coda	SA-355CT	0.03–10	○		○		alluvium	next to bank	Tech. Note, 64, PWRI
125	27.6	under overpass, long coda	SA-355CT	0.03–10	○		○		reclaimed	protecting works	Tech. Note, 64, PWRI
126	21.0	1F of 5-story building	SM-23						diluvium	flat	Tech. Note, 64, PWRI
127	39.9	about GL-25m(G1), in anchor and other side of bridge	SA-355		○				bedrock	in cliff	
128	1.1	trouble with UD component	VSE-11/12	0.014–40	○	UD	○	○	bedrock	gentle slope	
129	16.1	machine house next to school	VSE-11/12	0.014–40	○		○		alluvium	flat	
130	22.7		VSE-11/12	0.014–40	○		○		alluvium	plateau, flat	
131	24.6	1F of 3-story building	VSE-11/12	0.014–40	○				alluvium	flat	
132	25.6	1F of 2-story building	VSE-11/12	0.014–40	○		○		alluvium	flat	
133	28.0	1F of 2-story building	VSE-11/12	0.014–40	○		○		alluvium	flat	
134	30.0	1F of 3-story building	VSE-11/12	0.014–40	○		○		diluvium	flat	
135	45.3	on footing of gymnasium located on a hill top	VSE-11/12	0.014–40	○				bedrock	steep slope	
136	0.1		TG631		○		○		alluvium	flat	
137	5.1	liquefied ground	DAS320AV				○		alluvium	flat	
138	14.3		DAS320AV						reclaimed		
139	18.0	under step next to house	DAS320AV		○		○		reclaimed		

No.	Distance (km)	Situation	Instrument	Period Range	Wave	Saturate	Boring	PS log	Geology	Topography	Reference
140	18.8	in small machine house	TG631		○		○		diluvium	plateau, flat	
141	21.1	1F of 1-story building	DAS320AV						reclaimed		
142	24.5	1F of 1-story building	DAS320AV				○		reclaimed		
143	25.8		DAS320AV				○		alluvium	flat, near river	
144	26.0		DAS320AV				○		alluvium	flat	
145	26.1	1F of 2-story building	DAS314C				○		reclaimed		
146	28.5	Direction of TG631 is rotated 90 degrees.	TG631		○		○		alluvium	flat	
147	29.2		DAS320AV		○				alluvium	flat	
148	32.8	1F of 1-story building	DAS320AV				○		reclaimed		
149	32.8	1F of 1-story building	DAS320AV				○		diluvium	flat	
150	34.2	sensor table is isolated floor of building	DAS320AV		○		○		diluvium	flat	
151	35.8	NS component slightly rotates.	DAS320AV		○				diluvium	gentle slope	
152	36.6		TG631				○		alluvium	flat	
153	37.8		DAS320AV		○				alluvium	flat	
154	40.0	Direction of TG631 is rotating.	TG631		○				Neogene	gentle slope	
155	40.5	There are sensors of acc and vel.	DAS320AV & TG631		○				alluvium	flat	
156	42.7	direction of TG631 is rotating.	DAS320AV & TG631		○				alluvium	flat	
157	46.1		DAS320AV		○				alluvium	flat	
158	1.1	on weathered rock	VP-9462HHV		○		○	○	bedrock	bank between faults	
159	10.0		VP-9462HHV		○		○	○	reclaimed	flat	
160	11.1	other sensor of bore hole GL-25m,-97m	SDA-240	0.03–10	○		○	○	alluvium	flat	
161	17.9	other sensor of bore hole GL-1m and -70m	V401		○		○	○	reclaimed	flat	
162	28.7	Long has error of 1′.	SD-240	0.03–3.3	○		○		reclaimed	flat	
163	31.8	horizontal triangle array, B point is opened	VSE-11/12		○		○		alluvium	flat	
164	35.0	horizontal triangle array, B point is opened	VSE-11/12		○		○		diluvium	flat	
165	35.3	other sensor installed in bore hole and velocity type	PK-130H		○		○	○	bedrock	slope	
166	35.7	horizontal open cut of rock	SD203G.3		○		○		bedrock	flat	
167	48.8	other sensor in bore hole of GL-25m and -100m	SD-240	0.03–3.3	○		○	○	reclaimed	flat	
168	54.5	other sensor in bore hole of GL-20m	V-241FB		○		○	○	reclaimed	flat	
169	64.7		SD-240-3G		○		○		bank	steep slope	
170	78.1	GL-0, 10, 20m (GL = TP + 3.8m)	V-241FB		○		○		reclaimed	1 m bank	
171	85.7	on mat of reactor	SDA-240		○		○	○	bedrock	flat cut	
172	88.0		V-9462A		○		○	○	bank	on protection wall of 20 m	
173	91.3	on mat of reactor	SD-240		○			○	bedrock	flat	
174	102.8		VSE-11/12	0.014–40	○				bedrock	slope	
175	119.5	between turbine and reactor	PK-130		○			○	bedrock	flat	
176	55.9	on tunnel floor but isolated by sand	VSE-11/12	0.02–60	○				bedrock	slope	
177	64.5		VSE-11/12	0.02–60	○		○		alluvium	flat	
178	70.7		VSE-11/12	0.02–60	○				bedrock	slope	
179	80.9		VSE-11/12	0.02–60	○		○		alluvium	flat	
180	96.5		VSE-11/12	0.02–60	○		○		alluvium	flat	
181	112.6		VSE-11/12	0.02–60	○		○		alluvium	flat	
182	99.5	between school building	SA-355	0.03–10	○		○		alluvium	flat	
183	25.5	in tunnel under 60 m from surface	VSE-11/12		○				bedrock	steep slope	
184	58.3		VSE 11/12		○				bedrock	steep slope	

185	85.1		VSE 11/12		○				bedrock	steep slope	
186	115.6		VSE 11/12		○				bedrock	steep slope	
187	120.8		VSE 11/12		○				diluvium	steep slope	
188	35.8		VSE 11/12		○					flat	
189	21.7		VS3		○						
190	17.3	unknown because underground	PTK 130 HS/VS		○	EW	○		alluvium	garden	
191	20.8		DATOL-100		○		○		alluvium	flat	
192	22.0	dry area next to 5-story building	PTK 130 HS/VS		○		○		diluvium	GL-4m	
193	31.2	unknown because underground	DATOL-100		○				alluvium	flat	
194	32.8	unknown because underground	DATOL-100		○				diluvium	slope	
195	36.7	in house but on rock outcrop	SD240-3		○	EW			bedrock	gentle slope	
196	47.6				○				alluvium		
197	26.7	3 sensors on rock outcrop, on bank and under bank	SMAC-MD	0.03–50	○		○	○	bedrock	slope	
198	19.8		SMAC-MD		○		○	○			
199	80.3		SMAC-M		○		○		alluvium		
200	111.7		SMAC-MD		○				alluvium		
201	176.8		SMAC-MD		○		○				
202	19.8		SMAC-B2		○		○	○	diluvium	flat	Prompt Report 46, NIED
203	38.9						○			flat	
204	208.5								alluvium		
205	18.3	sensor installed 1, 15, 31F	SA-375 CT		○				diluvium	flat	
206	18.9	GL0m and −58m	VSE-11/12		○			○	alluvium	flat	
207	19.4	Gl-70.4, −28, −4m, 1, 20, 30, 41F	SA-156 CT		○			○	alluvium	flat	
208	24.5	1F of 5-story building	VSE-11/12		○				diluvium	flat	
209	17.9		SA-355 CT		○				alluvium	beside open cut	
210	19.4	other sensor is GL-60m, capacity is max 50 gal	PTK-130 H/V		○	EW	○		diluvium	flat	
211	36.4	other sensor is GL-100m, capacity is max 50 gal	PTK-130 H/V		○	NS,EW	○		diluvium	gentle slope	
212	0.5	1F in seriously damaged building	DAS-314				○		diluvium	gentle slope	
213	16.8	under elevated RW	DAS-314				○		alluvium	flat	
214	45.7	in machine house	DAS-314				○		alluvium	flat	
215	10.5	1F to 4-story building	SDA-240				○		alluvium	reclaimed	
216	7.7	under elevated RW	SDA-203				○		diluvium	gentle slope	
217	14.6	next to 4-story building	SM-40						bedrock	on protection works	
218	2.2	on liquefied soil	SD-240		○		○		reclaimed	flat	
219	14.2	on base of base isolation building	SDA-203		○		○	○	bedrock	flat	
220	14.5		SM-12V		○		○		bedrock	flat	
221	15.0	buried	SDA-203	0.03–10	○		○	○	alluvium	flat	
222	26.1	4 in runway, 1 at GL-50m	DATOL-200	0.02–40	○			○	reclaimed	flat	
223	0.7	1F of seriously damaged 4-story building	GTA40						diluvium	gentle slope	

*Japanese-style level designations: e.g., 1F, ground level; BIF is one level below ground. GL is free surface.
†max, composite of two horizontal components; LG and TR are parallel and orthogonal to structural apse line.